Atmos. Chem. Phys. Discuss., doi:10.5194/acp-2016-226, 2016
Manuscript under review for journal Atmos. Chem. Phys.
Published: 21 March 2016

Atmospheric Chemistry and Physics Discussions

Highly time-resolved urban aerosol characteristics during springtime in Yangtze River Delta, China: Insights from soot particle aerosol mass spectrometry

Junfeng Wang,[1] Xinlei Ge,[1,*] Yanfang Chen,[1] Yafei Shen,[1] Qi Zhang,[1,2] Yele Sun,[3] Jianzhong Xu,[4] Huan Yu,[1] Mindong Chen[1,*]

[1]Jiangsu Key Laboratory of Atmospheric Environment Monitoring and Pollution Control (AEMPC), Collaborative Innovation Center of Atmospheric Environment and Equipment Technology (CIC-AEET), School of Environmental Science and Engineering, Nanjing University of Information Science & Technology, Nanjing 210044, China

[2]Department of Environmental Toxicology, University of California at Davis, Davis, California 95616, United States

[3]State Key Laboratory of Atmospheric Boundary Layer Physics and Atmospheric Chemistry, Institute of Atmospheric Physics, Chinese Academy of Sciences, Beijing 100029, China

[4]State Key Laboratory of Cryospheric Sciences, Cold and Arid Regions, Environmental and Engineering Research Institute, Chinese Academy of Sciences, Lanzhou 730000, China

*Corresponding author, Email: caxinra@163.com; chenmdnuist@163.com

Phone: +86-25-58731394

For *Atmos. Chem. Phys.*

Atmos. Chem. Phys. Discuss., doi:10.5194/acp-2016-226, 2016
Manuscript under review for journal Atmos. Chem. Phys.
Published: 21 March 2016

Atmospheric Chemistry and Physics Discussions

Abstract: In this work, the Aerodyne soot particle – aerosol mass spectrometer (SP-AMS) was deployed for the first time during the spring of 2015 in urban Nanjing, a megacity in the Yangtze River Delta (YRD) of China, for online characterization of the submicron aerosols (PM_1). The SP-AMS enables real-time and fast quantification of refractory black carbon (*r*BC) simultaneously with other non-refractory species (ammonium, sulfate, nitrate, chloride and organics). The average PM_1 concentration was found to be 28.2 μg m^{-3} (~54% of the $PM_{2.5}$ mass), with organics (45%) as the most abundant component, following by sulfate (19.3%), nitrate (13.6%), ammonium (11.1%), *r*BC (9.7%) and chloride (1.3%). These PM_1 species together can reconstruct ~44% of the light extinction during this campaign based on the IMPROVE method. Chemically-resolved mass-based size distributions revealed that small particles especially ultrafine ones (<100 nm vacuum aerodynamic diameter) were dominated by organics and *r*BC, while large particles had significant contributions from secondary inorganic species. Source apportionment of organic aerosols (OA) yielded four OA subcomponents, including hydrocarbon-like OA (HOA), cooking-related OA (COA), semi-volatile oxygenated OA (SV-OOA), and low-volatility oxygenated OA (LV-OOA). Overall, secondary organic aerosol (SOA, equal to the sum of SV-OOA and LV-OOA) dominated the total OA mass (55.5%), but primary organic aerosol (POA, equal to the sum of HOA and COA) can outweigh SOA in early morning and evening due to enhanced human activities. High OA concentrations were often associated with high mass fractions of POA and *r*BC, indicating the important role of anthropogenic emissions during heavy pollution events. The diurnal cycles of nitrate, chloride and SV-OOA both showed good anti-correlations with air temperatures, suggesting their variations were likely driven by thermodynamic equilibria and gas-to-particle partitioning. On the other hand, in contrast to other species, sulfate and LV-OOA concentrations increased during afternoon, and showed no positive correlations with relative humidity (RH), indicating the significant role of photochemical processing rather than aqueous-phase processing for their formations. The bivariate polar plots show that the SV-OOA was formed locally, and the

Atmos. Chem. Phys. Discuss., doi:10.5194/acp-2016-226, 2016
Manuscript under review for journal Atmos. Chem. Phys.
Published: 21 March 2016

Atmospheric Chemistry and Physics Discussions

variations of hydrogen-to-carbon (H/C) and oxygen-to-carbon (O/C) ratios in the Van Krevelen space further suggests an evolution pathway of SV-OOA to LV-OOA. Our findings regarding springtime aerosol chemistry in Nanjing may have important implications for the air quality remediation in the densely populated regions.

1. Introduction

In recent years, high concentrations of fine particulate matter ($PM_{2.5}$) have been frequently observed (Hu et al., 2015), in accompanying with the visibility impairment and occurrence of haze events across large parts of China. $PM_{2.5}$ also affects human health (e.g., Pope and Dockery, 2006;Cao et al., 2012), regional and global climate (directly by absorbing and scattering solar radiation or indirectly by acting as cloud condensation nuclei and ice nuclei)(e.g.,Ghan and Schwartz, 2007;Pöschl, 2005), and the earth's ecosystem (Carslaw et al., 2010). These effects are predominantly dependent upon the physical and chemical characteristics of fine particles, such as mass concentration, chemical composition, size distribution, and hygroscopicity, all of which are influenced by the emission sources and transformation and evolution processes in the atmosphere.

The Yangtze River Delta (YRD) region is one of the most populated and economically developed areas in China, but it is also facing with severe air pollution lately. Nanjing, as one of the major megacities in this region, has a daily $PM_{2.5}$ mass concentration varying between 33-234 μg m^{-3} during November 2011 - August 2012, with an mean value of 106 μg m^{-3}, which is 4.2 times the WHO air quality standard of 25 μg m^{-3} (Shen et al., 2014). $PM_{2.5}$ pollution is significantly elevated during hazy days, for example, a daily average of 282 μg m^{-3} was observed for a heavily polluted day (Fu et al., 2008). A number of studies regarding aerosol chemistry in Nanjing have been conducted, and identified various inorganic components (sulfate, nitrate, ammonium and heavy metals, etc.) (e.g., Wang et al., 2003;Hu et al., 2012) and hundreds of organic species (carboxylic/dicarboxylic acids, amines and amino acids, polycyclic aromatic hydrocarbons, etc.) (Wang et al., 2011;Wang et al., 2002;Yang et

Atmos. Chem. Phys. Discuss., doi:10.5194/acp-2016-226, 2016
Manuscript under review for journal Atmos. Chem. Phys.
Published: 21 March 2016

al., 2005;Wang et al., 2009) that contribute to the aerosol mass. However, past studies mostly employed filter-based sampling technique, which due to low time resolution (a few hours to days), is often incapable of capturing details of the atmospheric evolution processes during the typical lifecycle of aerosols (Wexler and Johnston, 2008). Subsequent offline analyses may also introduce artifacts as some semi-volatile species can evaporate during sampling and storage (Dong et al., 2012).

On the other hand, in the past 15 years, the Aerodyne Aerosol Mass spectrometer (AMS) (Canagaratna et al., 2007) has been widely used, and was proven to be powerful for real-time online measurements of size-resolved chemical compositions of submicron aerosols (PM_1) with very fine time resolution (seconds to minutes) (Zhang et al., 2007a;Jimenez et al., 2009). The development of Aerodyne AMS began with the invention of quadruple AMS (Q-AMS) (Jayne et al., 2000), following by the compact time-of-flight AMS (C-ToF-AMS) (Drewnick et al., 2005), high resolution time-of-flight AMS (HR-ToF-AMS) (DeCarlo et al., 2006) and the soot particle AMS (SP-AMS) (Onasch et al., 2012). There are also an aerosol chemical speciation monitor (ACSM) (Ng et al., 2011) and its updated version of ToF-ACSM (Fröhlich et al., 2013), which are in particular designed for long-term unattended aerosol measurements. SP-AMS is the most advanced version, which in principle incorporates the single particle soot photometer (SP2) into the HR-ToF-AMS, and upgraded with a laser vaporizer for detecting refractory black carbon (*r*BC) and associated/coated species that cannot be measured by other types of AMS.

Recently, the Aerodyne AMS has been deployed widely in China (particularly Beijing) (e.g., Xu et al., 2014 and references therein;Sun et al., 2014;Yeung et al., 2014;Zhang et al., 2014;Li et al., 2015;Shen et al., 2015;Sun et al., 2015a;Sun et al., 2015b;Yan et al., 2015;Zhang et al., 2015;Tang et al., 2016;Zhang et al., 2016a;Jiang et al., 2015;Chen et al., 2015;Xu et al., 2015;Du et al., 2015;Sun et al., 2016;Wang et al., 2015;Han et al., 2015;Wang et al., 2016b). However, only a few field campaigns were conducted in the YRD region. Huang et al. (2012b) deployed an HR-ToF-AMS together with an SP2 in Shanghai during the 2010 Shanghai World Expo, and in

Atmos. Chem. Phys. Discuss., doi:10.5194/acp-2016-226, 2016
Manuscript under review for journal Atmos. Chem. Phys.
Published: 21 March 2016

Atmospheric Chemistry and Physics Discussions

Jiaxing during summer and winter of 2010 (Huang et al., 2012a). In urban Nanjing, an ACSM was applied for characterizing PM_1 during summer and autumn harvest seasons (Zhang et al., 2015), and during December 2013 to investigate a few heavy haze events (Zhang et al., 2016b). In addition, a Q-AMS was deployed in Nanjing to investigate the effects of PM_1 on visibility during January 2013 (Shen et al., 2015). Furthermore, a recent study by Wang et al. (2016a) reported the observation of fullerene soot in suburban Nanjing using an SP-AMS. Nevertheless, many questions remain with regard to aerosol chemistry, sources, and processes in this region. Moreover, none of the previous AMS measurements studied the aerosol characteristics during springtime in Nanjing. For these reasons, we reports in this work, for the first time, the real-time measurement results on urban fine aerosols in Nanjing using the SP-AMS during spring in 2015. The rich high resolution mass spectra (HRMS) data allow us to conduct in-depth analyses, and better understand the characteristics, sources and relevant transformation processes of ambient aerosols in Nanjing.

2. Experiments

2.1 Sampling site and instrumentation

The field campaign was conducted in the environment monitoring station of Nanjing Olympic center (32°0′33.00″N, 118°44′9.53″E, Fig. S1) from April 13 to 29, 2015. Details of the sampling site are shown in Fig. S1. The site was surrounded by residential buildings, close to a few urban arterial roads (~ 85 m northwest of Huangshan Road, ~ 200 m northeast to Mengdu Street and ~425 m southwest of Xinglong Street). There are also a restaurant (~50 m), a student cafeteria (~300 m), and the Nanjing Cigarette Factory (~480 m southeast) around the site.

The sampling inlet was installed outside the fifth floor of the building (~12 m above the ground), with a $PM_{2.5}$ cyclone (URG Corp., Chapel Hill, NC, USA) to remove coarse particles. Ambient particles were dried (RH <10%) via a diffusion dryer filled with silica gel before entering into the SP-AMS. The sampling line (~2 m

Atmos. Chem. Phys. Discuss., doi:10.5194/acp-2016-226, 2016
Manuscript under review for journal Atmos. Chem. Phys.
Published: 21 March 2016

Atmospheric Chemistry and Physics Discussions

144 long) was assembled using stainless steel tubing and proper fittings. Air flow was
145 controlled at around ~5 L min^{-1}, with a flow rate into the SP-AMS at ~80 cm^3 min^{-1}.
146 The SP-AMS can measure non-refractory (NR) PM_1 components including
147 ammonium, nitrate, sulfate, chloride and organics similar to other types of AMS via a
148 thermal tungsten heater. Moreover, it can also measure *r*BC and coated species as it is
149 equipped with an intracavity Nd:YAG laser vaporizer (1064 nm) (Onasch et al., 2012).
150 During this campaign, the instrument was switched between "laser on" and "laser off"
151 settings, and between V-mode (better for mass quantification) and W-mode (better
152 chemical resolution, ~5000 in this study), with one cycle including six menu settings
153 (M1: Laser on V-mode; M2: Laser off V-mode; M3: Laser on W-mode; M4: Laser off
154 W-mode; M7: Laser on PToF-mode; M8: Laser off PToF-mode). Each menu was set
155 to 2.5 min, thus a full running cycle lasted for 15 mins. The PToF-mode was under
156 V-mode, but was tuned in particular for measuring particle sizes. The tungsten heater
157 was always turned on and kept at ~600^{o}C.
158 The SP-AMS, in conjunction with a scanning mobility particle sizer (SMPS) (TSI
159 inc., Shoreview, MN, USA) was calibrated for mass quantification (e.g., ionization
160 efficiency) using size-selected (250 nm and 300 nm) monodisperse ammonium nitrate
161 particles following the procedures detailed in Jimenez et al. (2003). Pure ammonium
162 sulfate was used to determine the relative ionization efficiency (RIE) of sulfate
163 (Setyan et al., 2012). Quantification of *r*BC was calibrated using Regal Black
164 (REGAL 400R pigment black, Cabot Corp.) particles according to the procedures
165 reported in Onasch et al. (2012). Note that the solution of Regal Black was sonicated
166 during calibration to maintain a relative stable aerosol flow. RIEs of ammonium,
167 nitrate, sulfate, chloride, organics and *r*BC were determined to be 3.15, 1.05, 1.20, 1.3,
168 1.4 and 0.33, respectively. On the other hand, particle sizing was calibrated using
169 standard polystyrene latex (PSL) spheres (Duke Scientific Corp., Palo Alto, CA, USA)
170 across 100 - 700 nm range. Flow rate was also calibrated prior to the measurement.
171 Concentrations of gaseous species, e.g., carbon monoxide (CO) (Model T300,
172 Teledyne API, USA), ozone (O_3) (Model EC9810, Ecotech Pty Ltd, Australia),

Atmos. Chem. Phys. Discuss., doi:10.5194/acp-2016-226, 2016
Manuscript under review for journal Atmos. Chem. Phys.
Published: 21 March 2016

Atmospheric Chemistry and Physics Discussions

nitrogen dioxide (NO_2) and sulfur dioxide (SO_2) (Model LGH-01, Anhui Landun, China), and meteorological data including air temperature (T), relative humidity (RH), visibility (km), wind speed (WS) and wind direction (WD) were acquired at the same site. $PM_{2.5}$ and PM_{10} mass concentrations were also recorded (BAM-1020, Met One Instruments, Inc., USA), in parallel with the SP-AMS measurement.

2.2 Data treatment and source analyses

The SP-AMS data were post-processed by using the Igor-based standard ToF-AMS Analysis Toolkit SQUIRREL v1.56D and PIKA v1.15D, available at: http://cires1.colorado.edu/jimenez-group/ToFAMSResources/ToFSoftware/index.html. Note all mass concentrations reported here were calculated from the HR fitted results on V-mode data. A constant collection efficiency (CE) of 0.5 was used for the mass quantification, in consistent with many other AMS studies, as indeed the mass fraction of ammonium nitrate (mostly <40%), particle acidity (near neutral) and RH (<10%) do not affect the CE significantly for this dataset (Middlebrook et al., 2012).

Unless specified, the concentrations of ammonium, sulfate, nitrate, chloride and organics are from M2 setting (tungsten vaporizer only), while the *r*BC data is from M1 setting (dual-vaporizers: tungsten + laser) in this paper. The meteorological data (RH, T, WS, WD and visibility), concentrations of gas-phase species (CO, NO_2, SO_2 and O_3) and $PM_{2.5}$ were averaged into hourly data for comparisons with the SP-AMS data. The data reported are at local time, e.g., Beijing (BJ) Time.

Positive matrix factorization (PMF) (Paatero and Tapper, 1994) was applied on the HRMS of organic aerosol (OA) obtained under laser off W-mode (M4 setting) to elucidate the OA sources/processes. We used the PMF Evaluation Tool version 2.08A (downloaded from: http://cires1.colorado.edu/jimenez-group/wiki/index.php/PMF-AMS_Analysis_Guide) (Ulbrich et al., 2009) to investigate the PMF results by varying the number of factors (from 2 to 8 factors) and rotations ("*f*peak", from -1 to 1 with an increment of 0.1). Only ions with *m/z* less than or equal to 180 were included in the analyses. Following the instruction detailed by Zhang et al. (2011), the 4-factor solution (at *f*peak = -0.1)

Atmos. Chem. Phys. Discuss., doi:10.5194/acp-2016-226, 2016
Manuscript under review for journal Atmos. Chem. Phys.
Published: 21 March 2016

was chosen as the optimal solution, as the 3-factor solution cannot separate the hydrocarbon-like OA (HOA) and cooking OA (COA) (Fig. S2), and the 5-factor solution clearly splits the semi-volatile oxygenated OA (SV-OOA) factor into two OOA factors (Fig. S3). A summary of the key diagnostic plots are provided in Fig. S4. Detailed discussion of the PMF results is presented in Section 3.5. Note we found no significant differences between the PMF source apportionment results from the HRMS of OA obtained with dual-vaporizers setting (M3 setting) and current results (M4 setting, tungsten vaporizer only), as the OA HRMS acquired under these two circumstances were overall very similar (details in Section 3.4).

3. Results and discussion

3.1 Mass concentrations, chemical compositions and diurnal changes

The temporal variations of meteorological parameters, concentrations of the gas pollutants, concentrations and mass fractions of different PM_1 components, and the $PM_{2.5}$ mass loadings (from Met one BAM-1020) over the sampling period are illustrated in Fig. 1. During this study, the mean temperature was 18.5 ^oC, RH on average was 64%, and wind predominantly blew from southeast and southwest (Fig. S5). The SP-AMS PM_1 concentrations ranged from 5.1 to 97.9 μg m^{-3}, with an average of 28.2 μg m^{-3}. Note this average PM_1 concentration is significantly lower than those observed during summer (38.5 μg m^{-3}), autumn (46.4 μg m^{-3}) and winter (89.3 μg m^{-3}) (Zhang et al., 2015;Zhang et al., 2016b), showing that the air during springtime in Nanjing is cleaner than in other seasons. The variations of PM_1 concentrations also match very well with $PM_{2.5}$ concentrations (Pearson's $r^2 = 0.72$), and on average PM_1 accounts for ~ 54% of the $PM_{2.5}$ mass.

The average PM_1 composition is shown in Fig. 2a. The most abundant component is found to be organics (45.0%), following by sulfate (19.3%), nitrate (13.6%), ammonium (11.1%), *r*BC (9.7%) and chloride (1.3%). Fig. 2b further shows changes of the PM_1 chemical compositions in different concentration bins. It can be seen that although most PM_1 mass loadings are within 10 - 40 μg m^{-3}, high loading periods tend

Atmos. Chem. Phys. Discuss., doi:10.5194/acp-2016-226, 2016
Manuscript under review for journal Atmos. Chem. Phys.
Published: 21 March 2016

Atmospheric Chemistry and Physics Discussions

to have higher mass contributions from organics and *r*BC, and less contributions from secondary inorganic species, indicating that high PM events were influenced significantly by local fresh emissions.

The molar ratio of inorganic anions (sulfate, nitrate and chloride) to cations (ammonium) is 1.05 (Fig. 3a) (Zhang et al., 2007b). Considering that a small fraction of sulfate, nitrate and chloride are possibly associated with metal cations, such as Na^+, K^+ and Ca^{2+}, etc.，it can be concluded that the NR-PM_1 was overall neutral throughout the study. On the other hand, the molar ratio of inorganic anions to ammonium is on average 1.17 (Fig. 3b) when dual-vaporizers are on. This may be partially due to variations of ionization/collection efficiencies of the measured species as the addition of laser beam may change the distribution of vaporized species inside the ion chamber, and also because of the detection of sulfate, nitrate and chloride bonded with metal cations under the dual-vaporizers. These species don't evaporate on the tungsten vaporizer under the laser-off mode. Indeed, more metal signals were observed with the dual-vaporizers, as shown in Fig. S6.

Fig. 2c shows the average diurnal changes of organics, sulfate, nitrate, chloride and *r*BC. Sulfate concentrations are slightly higher during daytime than during nighttime, indicating a significant contribution from photochemical reactions. Sulfate also shows the least variations among all species, reflecting its regional behavior. Except for sulfate, all other species present a dual-peak pattern, with one peak in early morning and another one in early evening. The peaks of *r*BC and organics are likely due to local traffic/cooking activities (see details in Section 3.5), while the behavior of nitrate is likely driven by the thermodynamic gas-particle partitioning: $NH_4NO_3(p) \leftrightarrow NH_3(g) + HNO_3(g)$, as it shows good anti-correlations with the diurnal changes of temperatures (r = -0.72 for nitrate *vs.* T). Furthermore, we calculated the diurnal variations of the equilibrium constant of NH_4NO_3 ($K_{p,AN}$) (Young et al., 2015;Seinfeld and Pandis, 2006) in Fig. 2c. The $K_{p,AN}$ displays a similar trend as nitrate (r = 0.68), providing strong evidence that nitrate variations were governed mainly by the thermodynamic equilibrium. Chloride shows similar behavior as nitrate, indicating it

Atmos. Chem. Phys. Discuss., doi:10.5194/acp-2016-226, 2016
Manuscript under review for journal Atmos. Chem. Phys.
Published: 21 March 2016

Atmospheric Chemistry and Physics Discussions

is driven by the equilibrium $NH_4Cl(p) \leftrightarrow NH_3(g) + HCl(g)$, as well ($r$ = -0.76 for chloride *vs.* T). Therefore, when temperature rises, more NH_4NO_3 and NH_4Cl can dissociate into gaseous NH_3, HNO_3 and HCl, mass loadings of particle-phase nitrate and chloride decrease correspondingly, and *vice versa*.

In order to further elucidate the formation processes of nitrate and sulfate, we calculated the oxidation ratios of sulfur (f_S) and nitrogen (f_N) (Fig. 4a and 4b), defined as $f_S = nSO_4^{2-}/(nSO_4^{2-} + nSO_2)$ and $f_N = nNO_3^-/(nNO_3^- + nNO_2)$ (Xu et al., 2014), indicating the conversion of SO_2 and NO_2 to sulfate and nitrate, respectively. Here nSO_4^{2-}, nNO_3^-, nSO_2 and nNO_2 are the molar quantities of particle-phase sulfate and nitrate, gas-phase SO_2 and NO_2, respectively. Diurnal variations of f_S, f_N and mass ratios of SO_4^{2-}/NO_3^- are presented in Fig. 4d-f, along with the diurnal cycle of RH. The f_S reaches a maximum around 3 pm; similarly, the SO_4^{2-}/NO_3^- ratios are elevated significantly during daytime, in particular during afternoon. These behaviors suggest the remarkable role of photochemical processing of SO_2 to sulfate. In addition, the diurnal profile of f_S shows a negative correlation with that of RH (r = -0.52), indicating somewhat insignificant influence of aqueous-phase production of sulfate during this campaign. Interestingly, during nighttime (7 pm – 6 am), variations of f_N follows the changes of RH, probably suggesting a nighttime formation pathway of nitrate, e.g., $N_2O_5 + H_2O = 2HNO_3$ and $HNO_3 + NH_3 = NH_4NO_3$; while the afternoon drop of f_N is likely due to evaporation of nitrate as the temperature increases.

3.2 Chemically-resolved size distributions

The campaign-averaged mass-based size distributions, fractional contributions and diurnal size distributions (image plots) of the major PM_1 species are depicted in Fig. 5 (temporal variations of the mass-based size distributions of these PM_1 species over the whole measurement period are provided in Fig. S7). Note the size distribution of *r*BC in these plots were scaled from the size distribution of *m/z* 24 (C_2^+), as other major *r*BC ion clusters may be heavily influenced by other ions, such as C^+ signal but from organics at *m/z* 12 (C^+), HCl^+ signal at *m/z* 36 (C_3^+), SO^+ signal

Atmos. Chem. Phys. Discuss., doi:10.5194/acp-2016-226, 2016
Manuscript under review for journal Atmos. Chem. Phys.
Published: 21 March 2016

Atmospheric Chemistry and Physics Discussions

289 at *m/z* 48 (C_4^+), $C_2H_4O_2^+$ signal at *m/z* 60 (C_5^+). As can be expected, all inorganic
290 species (sulfate, nitrate, chloride and ammonium) display a unimodal distribution with
291 an accumulation mode peaking ~550 nm (vacuum aerodynamic diameter, D_{va}
292 (DeCarlo et al., 2004)), since they were mainly formed from secondary reactions. The
293 organics has a much broader size distribution across from ultrafine (<100 nm) to
294 supermicron meter range, with a small sub-peak centering ~120 nm in addition to the
295 major peak at ~440 nm, indicating influences from both primary and secondary
296 emissions. On the contrary, size distribution of *r*BC behaves very differently from
297 other components, which peaks at 90 - 200 nm range, reflecting clearly that it is
298 mainly originated from primary emissions. Overall, the small particles are
299 predominantly consisted of organics and *r*BC, which together account for more than
300 90% of the ultrafine particle mass. Mass contributions from inorganic species increase
301 significantly with the increase of particle size, and they dominate masses of particles
302 larger than 400 nm (Fig. 5b).

303 In line with the diurnal mass loadings of the PM_1 species shown in Fig. 2c, the
304 diurnal size distribution of sulfate is generally stable, with masses concentrating in the
305 400 - 700 nm range throughout the day (Fig. 5c); while the size distributions of nitrate,
306 chloride and organics present clear enhancements in the 300 - 700 nm range during
307 early morning and early evening due to increased mass concentrations of these species
308 during these two periods. The size distribution of *r*BC is also enhanced during the
309 morning and evening hours, but it extends to a much smaller size range (<100 nm).

310

311 **3.3 PM_1 contributions on visibility impairment**

312 In order to figure out the major species that are responsible for the visibility
313 degradation, here we employed the IMPROVE method to reconstruct the light
314 extinction coefficients (b_{ext}). b_{ext} values are derived from the measured visibility:
315 $b_{ext}=3.91/V_s$ (Kong et al., 2015), where V_s stands for the visibility (in meter). The
316 following IMPROVE formula (Yang et al., 2007) was used:

317 $$b_{ext} = 3f(RH)\{[(NH_4)_2SO_4] + [NH_4NO_3] + [NH_4Cl]\} + 4[OM] + 10[BC] + 1[soil]+10$$

Atmos. Chem. Phys. Discuss., doi:10.5194/acp-2016-226, 2016
Manuscript under review for journal Atmos. Chem. Phys.
Published: 21 March 2016

Atmospheric Chemistry and Physics Discussions

Where *f*(RH) is a RH-dependent empirical coefficient which considers the effects of water uptake by inorganic salts on the light extinction; the *f*(RH) values used here were taken from Malm and Day (2001), which were regressed from the Great Smoky data set. [$(NH_4)_2SO_4$], [NH_4NO_3], [NH_4Cl], [OM], and [BC] represent the mass concentrations of ammonium sulfate, ammonium nitrate, ammonium chloride, organics and black carbon directly from the SP-AMS measurements (in μg m^{-3}) ([$(NH_4)_2SO_4$] = 1.375*[SO_4^{2-}], [NH_4NO_3]=1.29*[NO_3^-] and [NH_4Cl] = 1.51*[Cl^-]). Since the SP-AMS cannot accurately measure soil components (e.g., various metals/metal oxides/metal salts), the term [soil] was set to zero during calculations.

By using this method, the reconstructed visibilities match reasonably well with the measured values (r^2 = 0.50) as shown in Fig. 6a. Fig. 6b shows the time series of the measured and reconstructed extinction coefficients throughout the whole sampling period. It should be noted that, on average, the measured PM_1 species are only able to explain ~44% of the light extinction. This is likely due to that: 1) as shown earlier, the SP-AMS measured PM_1 only occupies ~54% of the $PM_{2.5}$ mass; 2) we didn't include contributions from soil components, coarse particles and also some gas-phase species (such as NO_2); 3) although the influences of water are included in part through *f*(RH) for inorganic salts, the water uptake by organic species are not considered explicitly, which can be significant especially for the SOA under high RH conditions (Duplissy et al., 2011;Denjean et al., 2015). Indeed, as shown in Fig. 6a, reconstructed visibilities appear to deviate more significantly from the measured visibilities under high RH than ones under low RH conditions, suggesting the importance of particle-bounded water on visibility degradation. The pie chart in Fig. 6b presents the average relative contributions of different components to the light extinction of PM_1. The largest contributor is organics which accounts for 37.7%, followed by ammonium sulfate (25.1%), *r*BC (20.7%), ammonium nitrate (15.1%) and a minor contributor of ammonium chloride (1.4%).

3.4 Chemical characteristics of OA

Atmos. Chem. Phys. Discuss., doi:10.5194/acp-2016-226, 2016
Manuscript under review for journal Atmos. Chem. Phys.
Published: 21 March 2016

Atmospheric Chemistry and Physics Discussions

The unique laser vaporizer of SP-AMS allows it to detect *r*BC and species coated on the *r*BC core including both non-refractory and refractory organics, thus comparison between the OA mass spectra obtained with dual-vaporizers and tungsten vaporizer settings, can infer some information regarding the chemical features of refractory organics, that were unable to be determined by any other types of AMS. As shown in Fig. 7a and 7b, the OA obtained with dual-vaporizers setting have slightly higher oxygen-to-carbon (O/C) ratio (0.28 *vs.* 0.27), nitrogen-to-carbon (N/C) ratio (0.033 *vs.* 0.032) and lower hydrogen-to-carbon (H/C) ratio (1.50 *vs.* 1.52) than the corresponding elemental ratios of OA obtained with the tungsten vaporizer only. This result indicates that refractory organics are likely more oxygenated than the non-refractory organics, and for this dataset it is mainly due to a higher fractional contribution from $C_2H_3O^+$ (see the inset of Fig. 7a). This is different from the results on laboratory-generated nascent soot, where larger fCO_2^+ (i.e., the fraction of total organic signal contributed by CO_2^+) was observed with the dual-vaporizers setting, indicating the variability of the chemical compositions of refractory organics. Note the elemental ratios shown throughout the paper were all calculated based on the method proposed by Aiken et al. (2008) (referred to as A-A method). Recently, Canagaratna et al. (2015) improved this methodology by using specific ion fragments as markers to calculate the O/C and H/C ratios (referred to as I-A method). The I-A method increased the O/C ratio, H/C ratio, and the OM/OC ratio higher than the values calculated from the the A-A method, on average, by 28%, 10% and 8%, respectively (Fig. S8). In this work, we used the results from the A-A method for consistency and comparisons with previous AMS measurements.

Overall, the O/C ratio (0.27) of OA in Nanjing during springtime is a bit lower than those observed at other urban locations in China – for instances, 0.30 in Shenzhen (He et al., 2011), 0.31 in Shanghai (Huang et al., 2012b), 0.33 in Lanzhou (Xu et al., 2014) and 0.34 in Beijing (Zhang et al., 2014), and much lower than those at rural sites – for instances, 0.47 in Kaiping (Huang et al., 2011) and 0.59 in Changdao (Hu et al., 2013). As O/C ratio is a good indicator of the aging degree of

Atmos. Chem. Phys. Discuss., doi:10.5194/acp-2016-226, 2016
Manuscript under review for journal Atmos. Chem. Phys.
Published: 21 March 2016

Atmospheric Chemistry and Physics Discussions

OA, the relatively low O/C level indicates a significant contribution from fresh emissions in Nanjing aerosols during springtime. Accordingly, the non-refractory OA (pie chart in Fig. 7b) is dominated in hydrocarbon $C_xH_y^+$ ions (51.2%) rather than the oxygen-containing ion fragments (37.4% of $C_xH_yO_1^+$ and $C_xH_yO_2^+$).

The scatter plot of *f*44 (mass fraction of *m/z* 44 to the total OA) *vs.* *f*43 (mass fraction of *m/z* 43 to the total OA) (a.k.a., triangle plot) (Ng et al., 2010) was often used to investigate the oxidation degrees of OA. As presented in Fig. 8, most OA reside in the bottom end of the triangular region, again pointing out the less-oxygenated behavior of the OA. Since the HRMS can separate different ions at the nominal *m/z*, we also examined the fCO_2^+ *vs.* $fC_2H_3O^+$ space and illustrated it in Fig. S9 - many OA locate outside the triangular region, yet still close to the bottom. Moreover, *m/z* 60 (mainly $C_2H_4O_2^+$) is a significant fragment ion of levoglucosan, which is well known as the biomass burning aerosol tracer (Alfarra et al., 2007). However, as *f*60 (mass fraction of *m/z* 60 to the total OA) is very low in OA (average $\pm$ 1σ = 0.4 $\pm$ 0.06 %), indicating no biomass burning influences on the OA properties during springtime in Nanjing.

3.5 Sources and evolution processes of OA

In order to further elucidate the sources and evolution processes of OA, we performed PMF analyses and identified four OA components, including two primary OA (POA) factors – a traffic-related hydrocarbon-like OA (HOA) and a cooking-related OA (COA), and two secondary OA factors – a semi-volatile oxygenated OA (SV-OOA) and a low volatility OOA (LV-OOA). Details about their characteristics are discussed below.

3.5.1 Mass spectral features of the OA factors

The mass spectral profiles, time-dependent mass concentrations of the four OA factors and corresponding tracer ions are presented in Fig. 9. The HOA mass spectrum is overall dominated by the $C_xH_y^+$ ions (73.2%), such as $C_3H_7^+$, $C_4H_7^+$, $C_4H_9^+$, $C_5H_9^+$ etc., which are most likely produced from alkanes and cycloalkanes emitted from fuel

Atmos. Chem. Phys. Discuss., doi:10.5194/acp-2016-226, 2016
Manuscript under review for journal Atmos. Chem. Phys.
Published: 21 March 2016

Atmospheric Chemistry and Physics Discussions

and lubricating oil burning (Canagaratna et al., 2004). This feature is in good agreement with the mass spectral features of POA directly from vehicle emissions(Collier et al., 2015), and the HOA factors determined in many other locations (e.g., Ge et al., 2012b;Huang et al., 2010;Sun et al., 2011). HOA has the lowest O/C ratio (0.10) and highest H/C ratio (1.75) among all factors, representing its behavior as primary fresh emissions. The COA mass spectrum is also rich in $C_xH_y^+$ ions (64.7%), but having more oxygenated ions ($C_xH_yO_z^+$) than the HOA (26.5% *vs.* 15.4%), especially $C_3H_3O^+$ and $C_3H_5O^+$ ions. The significant contributions of $C_3H_3O^+$ and $C_3H_5O^+$ to *m/z* 55 and *m/z* 57 are a common feature of COA, that has been reported in various urban locations around the world, for examples, Beijing (Sun et al., 2015a), London (Allan et al., 2010), Fresno (Ge et al., 2012b), New York City (Sun et al., 2011) and Barcelona (Mohr et al., 2012;Mohr et al., 2015). These oxygen-containing ions are in part generated from the fragmentation of fatty acids in the cooking aerosols (Ge et al., 2012b). As a result, COA has a higher O/C ratio of 0.16 and a lower H/C ratio of 1.67 than those of HOA. The O/C and H/C levels of COA in this work are also close to those identified in other locations aforementioned. The consistency of the chemical characteristics of COA from such different locations suggests that ambient COA is more relevant to the cooking oil rather than the different types of food, which was postulated earlier by Allan et al. (2010).

Unlike the two POA factors, SV-OOA and LV-OOA are both abundant in oxygen-containing fragments ($C_xH_yO_z^+$ ions), which are 46.4% and 54.8%, respectively. The higher O/C ratio (0.55 *vs.* 0.32) and more $C_xH_yO_2^+$ ions (18.8% *vs.* 11.8%) in the LV-OOA mass spectrum than those of the SV-OOA, reflecting the fact that LV-OOA went through more aging/oxidation reactions than the SV-OOA. The O/C ratio of SV-OOA is 0.32, which is within the O/C range of SV-OOA observed worldwide (Jimenez et al., 2009). The LV-OOA O/C ratio of 0.55 is in the lower end compared to the O/C levels of LV-OOA observed in other China sites, for examples, 0.64 in Kaiping (Huang et al., 2011), 0.65 in Shanghai (Huang et al., 2012b), 0.68 in Lanzhou (Xu et al., 2014), 0.78 in Changdao (Hu et al., 2013) and 0.80 in Hong Kong

Atmos. Chem. Phys. Discuss., doi:10.5194/acp-2016-226, 2016
Manuscript under review for journal Atmos. Chem. Phys.
Published: 21 March 2016

Atmospheric Chemistry and Physics Discussions

(Lee et al., 2013).

Consistently, in the *f*44 *vs.* *f*43 space (Fig. 8), SV-OOA situates near the bottom side while LV-OOA approaches to the upper part of the triangular region, because of a much larger fractional contribution of CO_2^+ in the LV-OOA mass spectrum. HOA and COA, as POA factors, both reside in the bottom end of the plot, away from SV-OOA and LV-OOA; while they locate outside the triangle in the fCO_2^+ *vs.* $fC_2H_3O^+$ space (Fig. S9), indicating that the HRMS acquired by the SP-AMS is better in differentiating POA factors from other SOA factors than the unit mass resolution (UMR) data.

In order to justify the OA factors identified in this study, we compared the spectral similarities of the OA factor spectral profiles (in both HR and UMR) with those separated during wintertime in Beijing (Sun et al., 2015a), summertime in Lanzhou (Xu et al., 2014), and wintertime in Fresno (Ge et al., 2012b;Ge et al., 2012a). The results are listed in Table 1. Indeed, the HOA, COA and LV-OOA mass spectra are highly similar to the corresponding factors identified in Bejing, Lanzhou and Fresno ($r^2 > 0.87$); SV-OOA also correlates fairly well with Bejing and Lanzhou SV-OOA too, but with relative low r^2 (0.68 – 0.75), mainly because of one or two ion fragments, namely, higher CO^+ and CO_2^+ signals in Beijing SV-OOA and higher $C_2H_3O^+$ signal in Lanzhou SV-OOA than those in Nanjing SV-OOA. The SV-OOA on the other hand, correlates very well with the Fresno OOA ($r^2 = 0.90$ and 0.91).

Moreover, as presented in Fig. 9a, the HOA mass spectrum contains relatively higher fraction of ions with large *m/z* values (*m/z* > 100) than that of COA (14.0% *vs.* 8.2%), and most of these ions are $C_xH_y^+$ ions, probably from fuel burning emitted long-chain alkanes, etc. The SV-OOA also includes more large *m/z* ion fragments (*m/z*> 100) than those in the LV-OOA mass spectrum (10.5% *vs.* 5.3%), likely suggesting that further oxidation of SOA species may lead to the fragmentation of high molecular weight species and formation of small molecules – a mechanism verified by both lab-scale experiments (e.g., Yu et al., 2014) and field measurements (e.g., Lee et al., 2012).

Atmos. Chem. Phys. Discuss., doi:10.5194/acp-2016-226, 2016
Manuscript under review for journal Atmos. Chem. Phys.
Published: 21 March 2016

Atmospheric Chemistry and Physics Discussions

463 **3.5.2 Temporal variations, diurnal patterns and relative contributions of the OA**
464 **factors**

465 The temporal variations of different OA factors and their corresponding tracer
466 ions are displayed in Fig. 9b. $C_4H_9^+$ ion, a.k.a., the HOA mass spectral tracer (Zhang
467 et al., 2005) indeed varies very closely to the HOA (r^2= 0.94). Time series of the COA
468 tracer ion $C_6H_{10}O^+$ (and also $C_5H_8O^+$, $C_7H_{12}O^+$) (Sun et al., 2011;Ge et al., 2012b)
469 match very well with that of COA too (r^2 = 0.90). SV-OOA correlates better with
470 $C_2H_3O^+$ (r^2 = 0.90) than with CO_2^+ (r^2 = 0.66). Although LV-OOA doesn't correlate
471 very well with CO_2^+ (r^2 = 0.12) mainly due to the mismatch during April 23 - 26, the
472 correlation is still much better than it with $C_2H_3O^+$ (r^2 < 0.001). In Table 2, we
473 tabulate the correlation coefficients (r) of the four OA factors with the gas-phase
474 species, BC and inorganic species. Note we used Pearson's r not r^2 here since some
475 correlation coefficients are negative. From the table, it is clear that the traffic-related
476 gaseous species, CO and NO_2, correlate best with HOA among all OA factors;
477 SV-OOA correlates better with nitrate (r = 0.49) than it with sulfate (r = 0.11);
478 LV-OOA correlate better with sulfate (r = 0.23) that it with nitrate (r = 0.11). All these
479 results are consistent with the traffic origin of HOA, the semi-volatile and
480 low-volatility behaviors of SV-OOA and LV-OOA.

481 Accordingly, diurnal cycles of the OA factors are presented in Fig. 10a.
482 Correlation coefficients (r) of the diurnal variations between OA factors with
483 gas-phases and inorganic species are provided in Table 2, as well. HOA
484 concentrations show an early morning peak, and it overall remains at high levels
485 during nighttime. Besides the impacts of boundary layer height, this is also due to
486 enhanced emissions from construction vehicles around the site, which were in fact
487 much more active during nighttime than during daytime because of the restrictions of
488 Nanjing government. Most of those vehicles used low-quality diesel fuel, and could
489 emit a large amount of *r*BC particles. The *r*BC diurnal pattern is indeed almost
490 identical to that of HOA (r =0.99), indicating that the HOA during this campaign was
491 apparently associated with the construction vehicle emissions. COA concentrations

Atmos. Chem. Phys. Discuss., doi:10.5194/acp-2016-226, 2016
Manuscript under review for journal Atmos. Chem. Phys.
Published: 21 March 2016

492 increase during noon (12 pm – 1 pm) and early evening, in response to the lunchtime
493 and dinnertime cooking activities. SV-OOA concentrations decreases from 9 am, and
494 reach a minimum during afternoon (3 pm – 4 pm), oppositely to the variation of
495 temperatures (r = -0.85) but similar to that of nitrate (r = 0.53), corroborating its
496 semi-volatile feature. Different from other factors, LV-OOA concentrations increase
497 during daytime and shows positive correlation with temperature (r = 0.76); it also has
498 negative correlation with the diurnal cycle of RH (r = -0.75). Both behaviors are
499 similar to those of sulfate (r = 0.72 for the diurnal cycle of LV-OOA *vs.* sulfate),
500 indicating the leading role of photochemical oxidation for LV-OOA formation as well.
501 As shown in Fig. 10b, due to mainly the increase of LV-OOA mass loading, OA is
502 overwhelmingly dominated by the SOA (SV-OOA + LV-OOA) during afternoon (80.2%
503 at 3 pm); POA (HOA + COA) only dominates the OA mass during morning (53.2% at
504 7 am) and early evening (56.9% at 8 pm) in response to the enhanced traffic and
505 cooking emissions. On average, the OA is composed of 27.6% of HOA, 16.9% of
506 COA, 27.4% of SV-OOA and 28.1% of LV-OOA (Fig. 10c), with SOA outweighing
507 POA (55.5% *vs.* 44.5%). However, as shown in Fig. 10d, with the increase of OA
508 mass loadings, the fractional contribution of POA increases, highlighting the
509 important and direct influences of anthropogenic emissions on the heavy pollution
510 haze events.
511
512 **3.5.3 Local/regional influences and evolution processes of the OA factors**
513 Combining WS, WD and mass loadings, the bivariate polar plots of the four OA
514 factors, *r*BC, and total PM_1 are shown in Fig. 11. These plots provide an effective
515 graphical method for showing the potential influences of air masses from different
516 directions with different wind speeds to the receptor site (Carslaw and Beevers, 2013).
517 Clearly, high mass loadings of HOA and *r*BC mostly link with low WS (< 1 m s^{-1}),
518 indicating they are mainly from local vehicle emissions. High COA concentrations
519 occur mainly under low WS as well, but with some high concentrations accompanied
520 with air masses from southeast under higher WS. SV-OOA appears to be formed

Atmos. Chem. Phys. Discuss., doi:10.5194/acp-2016-226, 2016
Manuscript under review for journal Atmos. Chem. Phys.
Published: 21 March 2016

521 locally, except for a concentration hotspot in the southeast – likely due to emissions
522 from the tobacco factory that resides in that direction. High concentrations of
523 LV-OOA are distributed in all directions under higher WS, representing its regional
524 behaviors. Overall, high PM_1 mass loadings occur mainly under low WS, indicating
525 that the PM_1 is heavily affected by local emissions rather than pollutants in a regional
526 scale.

527 The aging of OA can be described in general by the increase of O/C and decrease
528 of H/C. In this regard, we plotted the Van Krevelen diagram (Heald et al., 2010) (Fig.
529 12a) to show the relationships between H/C and O/C ratios for all OA as well as the
530 four OA factors. Overall, in this study, the H/C and O/C ratios of OA data are
531 correlated linearly with a slope of -1.04 (r^2 = 0.93), indicating the propagation of OA
532 is similar to an aging process that is likely driven by the addition of carboxylic acid
533 (slope of -1). Interestingly, the two OOA factors lie very well on the fitted straight line.
534 This trend may suggest that the evolution of secondary OA during this campaign
535 follows a transformation pathway of SV-OOA to LV-OOA through the addition of
536 carboxylic acid. The diurnal cycle of LV-OOA varies oppositely to that of SV-OOA (r
537 = -0.86), probably supporting this hypothesis. In addition, O/C ratios of OA show no
538 obvious correlation with the RH as shown in Fig. 12b, verifying that aqueous-phase
539 processing is insignificant compared to the photochemical processing for the
540 oxidation of OA.
541
542 **4. Conclusions**
543 We present for the first time the real-time measurement results using the SP-AMS
544 on submicron aerosols in urban Nanjing during springtime (April 13 - 29, 2015). The
545 SP-AMS determined PM_1 mass loadings, agreed well with the $PM_{2.5}$ concentrations
546 measured by the Met One $PM_{2.5}$ analyzer. The average PM_1 concentration was 28.2 μg
547 m^{-3}, lower than previously ACSM-determined PM_1 concentrations during summer and
548 winter in Nanjing. Organics on average comprised the largest fraction (45%) of PM_1,
549 and its fractional contributions increased in case of high PM_1 mass loadings. The

Atmos. Chem. Phys. Discuss., doi:10.5194/acp-2016-226, 2016
Manuscript under review for journal Atmos. Chem. Phys.
Published: 21 March 2016

Atmospheric Chemistry and Physics Discussions

diurnal cycles of mass concentrations of organics, *r*BC, nitrate and chloride all presented a similar behavior, which was high in early morning and evening, but low in the afternoon. Concentrations of sulfate, on the contrary, increased during afternoon. Further investigations of f_S, f_N, SO_4^{2-}/NO_3^- and RH revealed that photochemical processing contributed significantly to sulfate formation, while nitrate (and chloride) formation was mainly governed by the thermodynamic equilibrium. The chemically-resolved mass-based size distribution data showed that *r*BC occupied a large fraction of ultrafine particles, while secondary inorganic species could dominate the mass of particles larger than 400 nm (D_{va}). In addition, by using the IMPROVE method, we found that the observed PM_1 components were able to reproduce ~44% of the light extinction during this study.

PMF analyses resolved four OA factors, e.g., HOA, COA, SV-OOA and LV-OOA. Mass spectral profiles of these factors agree very well with the corresponding factors identified at other locations. The springtime OA showed no influences from biomass burning emissions. On average, the OA is dominated by SOA (55.5%), but POA appeared to be more important when the OA mass loadings are high, and can be dominant in early morning and evening. Diurnal cycle of SV-OOA varied similarly to that of nitrate, reflecting its semi-volatile behavior. Diurnal variations of LV-OOA showed great resemblance to that of sulfate, indicating its formation was mainly from photochemical oxidation, as well. The bivariate polar plots indicate that SV-OOA was formed locally, and the Van Krevelen diagram further suggests a transformation pathway of SV-OOA to LV-OOA probably via the addition of carboxylic acid. Generally, our highly time-resolved SP-AMS measurement results may offer useful insights into the aerosol chemistry, and have important implications for the PM control and reduction in this densely populated region.

Acknowledgements

This work was supported by the Natural Science Foundation of China (Grant Nos. 21407079 and 91544220), the Jiangsu Natural Science Foundation (BK20150042),

the Jiangsu Provincial Specially-Appointed Professors Foundation, the Jiangsu Innovation and Entrepreneurship Program, the Startup Foundation for Introducing Talent of NUIST (2014r064), and the LAPC Open Fund (LAPC-KF-2014-06). M. Chen also acknowledges the support from the Natural Science Foundation of China (Grant Nos. 21577065 and 91543115), the Commonweal Program of Environment Protection Department of China (201409027-05), and the International ST Cooperation Program of China (2014DFA90780). The authors thank Nanjing Environmental Monitoring Center for the supporting data, and the help from Shun Ge, Ling Li, Yanan He, Hui Chen and Yangzhou Wu during the campaign and preparation of the manuscript.

References

Aiken, A. C., Decarlo, P. F., Kroll, J. H., Worsnop, D. R., Huffman, J. A., Docherty, K. S., Ulbrich, I. M., Mohr, C., Kimmel, J. R., Sueper, D., Sun, Y., Zhang, Q., Trimborn, A., Northway, M., Ziemann, P. J., Canagaratna, M. R., Onasch, T. B., Alfarra, M. R., Prevot, A. S. H., Dommen, J., Duplissy, J., Metzger, A., Baltensperger, U., and Jimenez, J. L.: O/C and OM/OC ratios of primary, secondary, and ambient organic aerosols with high-resolution time-of-flight aerosol mass spectrometry, Environ. Sci. Technol., 42, 4478-4485, 10.1021/Es703009q, 2008.

Alfarra, M. R., Prevot, A. S. H., Szidat, S., Sandradewi, J., Weimer, S., Lanz, V. A., Schreiber, D., Mohr, M., and Baltensperger, U.: Identification of the Mass Spectral Signature of Organic Aerosols from Wood Burning Emissions, Environ. Sci. Technol., 41, 5770-5777, 10.1021/es062289b, 2007.

Allan, J. D., Williams, P. I., Morgan, W. T., Martin, C. L., Flynn, M. J., Lee, J., Nemitz, E., Phillips, G. J., Gallagher, M. W., and Coe, H.: Contributions from transport, solid fuel burning and cooking to primary organic aerosols in two UK cities, Atmos. Chem. Phys., 10, 647-668, 10.5194/acp-10-647-2010, 2010.

Canagaratna, M. R., Jayne, J. T., Ghertner, D. A., Herndon, S., Shi, Q., Jimenez, J. L., Silva, P. J., Williams, P., Lanni, T., Drewnick, F., Demerjian, K. L., Kolb, C. E., and Worsnop, D. R.: Chase studies of particulate emissions from in-use New York City vehicles, Aerosol Sci. Tech., 38, 555-573, 10.1080/02786820490465504, 2004.

Canagaratna, M. R., Jayne, J. T., Jimenez, J. L., Allan, J. D., Alfarra, M. R., Zhang, Q., Onasch, T. B., Drewnick, F., Coe, H., Middlebrook, A., Delia, A., Williams, L. R., Trimborn, A. M., Northway, M. J., DeCarlo, P. F., Kolb, C. E., Davidovits, P., and Worsnop, D. R.: Chemical and microphysical characterization of ambient aerosols with the aerodyne aerosol

614 mass spectrometer, Mass Spectrom. Rev., 26, 185-222, 10.1002/Mas.20115, 2007.

615 Canagaratna, M. R., Jimenez, J. L., Kroll, J. H., Chen, Q., Kessler, S. H., Massoli, P.,
616 Hildebrandt Ruiz, L., Fortner, E., Williams, L. R., Wilson, K. R., Surratt, J. D., Donahue, N.
617 M., Jayne, J. T., and Worsnop, D. R.: Elemental ratio measurements of organic compounds
618 using aerosol mass spectrometry: characterization, improved calibration, and implications,
619 Atmos. Chem. Phys., 15, 253-272, 10.5194/acp-15-253-2015, 2015.

620 Cao, J. J., Xu, H. M., Xu, Q., Chen, B. H., and Kan, H. D.: Fine Particulate Matter
621 Constituents and Cardiopulmonary Mortality in a Heavily Polluted Chinese City, Environ.
622 Health Persp., 120, 373-378, 10.1289/ehp.1103671, 2012.

623 Carslaw, D. C., and Beevers, S. D.: Characterising and understanding emission sources using
624 bivariate polar plots and k-means clustering, Environ. Model. Soft., 40, 325-329,
625 10.1016/j.envsoft.2012.09.005, 2013.

626 Carslaw, K. S., Boucher, O., Spracklen, D. V., Mann, G. W., Rae, J. G. L., Woodward, S., and
627 Kulmala, M.: A review of natural aerosol interactions and feedbacks within the Earth system,
628 Atmos. Chem. Phys., 10, 1701-1737, 10.5194/acp-10-1701-2010, 2010.

629 Chen, C., Sun, Y. L., Xu, W. Q., Du, W., Zhou, L. B., Han, T. T., Wang, Q. Q., Fu, P. Q., Wang,
630 Z. F., Gao, Z. Q., Zhang, Q., and Worsnop, D. R.: Characteristics and sources of submicron
631 aerosols above the urban canopy (260 m) in Beijing, China, during the 2014 APEC summit,
632 Atmos. Chem. Phys., 15, 12879-12895, 10.5194/acp-15-12879-2015, 2015.

633 Collier, S., Zhou, S., Kuwayama, T., Forestieri, S., Brady, J., Zhang, M., Kleeman, M., Cappa,
634 C., Bertram, T., and Zhang, Q.: Organic PM Emissions from Vehicles: Composition, O/C
635 Ratio, and Dependence on PM Concentration, Aerosol Sci. Tech., 49, 86-97,
636 10.1080/02786826.2014.1003364, 2015.

637 DeCarlo, P. F., Slowik, J. G., Worsnop, D. R., Davidovits, P., and Jimenez, J. L.: Particle
638 morphology and density characterization by combined mobility and aerodynamic diameter
639 measurements. Part 1: Theory, Aerosol Sci. Tech., 38, 1185-1205,
640 10.1080/02786820590928897, 2004.

641 DeCarlo, P. F., Kimmel, J. R., Trimborn, A., Northway, M. J., Jayne, J. T., Aiken, A. C., Gonin,
642 M., Fuhrer, K., Horvath, T., Docherty, K. S., Worsnop, D. R., and Jimenez, J. L.:
643 Field-deployable, high-resolution, time-of-flight aerosol mass spectrometer, Anal. Chem., 78,
644 8281-8289, 10.1021/Ac061249n, 2006.

645 Denjean, C., Formenti, P., Picquet-Varrault, B., Pangui, E., Zapf, P., Katrib, Y., Giorio, C.,
646 Tapparo, A., Monod, A., Temime-Roussel, B., Decorse, P., Mangeney, C., and Doussin, J. F.:
647 Relating hygroscopicity and optical properties to chemical composition and structure of
648 secondary organic aerosol particles generated from the ozonolysis of α-pinene, Atmos. Chem.
649 Phys., 15, 3339-3358, 10.5194/acp-15-3339-2015, 2015.

650 Dong, H. B., Zeng, L. M., Hu, M., Wu, Y. S., Zhang, Y. H., Slanina, J., Zheng, M., Wang, Z.
651 F., and Jansen, R.: Technical Note: The application of an improved gas and aerosol collector
652 for ambient air pollutants in China, Atmos. Chem. Phys., 12, 10519-10533,
653 10.5194/acp-12-10519-2012, 2012.

654 Drewnick, F., Hings, S. S., DeCarlo, P., Jayne, J. T., Gonin, M., Fuhrer, K., Weimer, S.,
655 Jimenez, J. L., Demerjian, K. L., Borrmann, S., and Worsnop, D. R.: A new time-of-flight
656 aerosol mass spectrometer (TOF-AMS) - Instrument description and first field deployment,
657 Aerosol Sci. Tech., 39, 637-658, 10.1080/02786820500182040, 2005.

658 Du, W., Sun, Y. L., Xu, Y. S., Jiang, Q., Wang, Q. Q., Yang, W., Wang, F., Bai, Z. P., Zhao, X.
659 D., and Yang, Y. C.: Chemical characterization of submicron aerosol and particle growth
660 events at a national background site (3295 m a.s.l.) on the Tibetan Plateau, Atmos. Chem.
661 Phys., 15, 10811-10824, 10.5194/acp-15-10811-2015, 2015.

662 Duplissy, J., DeCarlo, P. F., Dommen, J., Alfarra, M. R., Metzger, A., Barmpadimos, I., Prevot,
663 A. S. H., Weingartner, E., Tritscher, T., Gysel, M., Aiken, A. C., Jimenez, J. L., Canagaratna,
664 M. R., Worsnop, D. R., Collins, D. R., Tomlinson, J., and Baltensperger, U.: Relating
665 hygroscopicity and composition of organic aerosol particulate matter, Atmos. Chem. Phys., 11,
666 1155-1165, 10.5194/acp-11-1155-2011, 2011.

667 Fröhlich, R., Cubison, M. J., Slowik, J. G., Bukowiecki, N., Prévôt, A. S. H., Baltensperger,
668 U., Schneider, J., Kimmel, J. R., Gonin, M., Rohner, U., Worsnop, D. R., and Jayne, J. T.: The
669 ToF-ACSM: a portable aerosol chemical speciation monitor with TOFMS detection, Atmos.
670 Meas. Tech., 6, 3225-3241, 10.5194/amt-6-3225-2013, 2013.

671 Fu, Q. Y., Zhuang, G. S., Wang, J., Xu, C., Huang, K., Li, J., Hou, B., Lu, T., and Streets, D.
672 G.: Mechanism of formation of the heaviest pollution episode ever recorded in the Yangtze
673 River Delta, China, Atmos. Environ., 42, 2023-2036, 10.1016/j.atmosenv.2007.12.002, 2008.

674 Ge, X., Zhang, Q., Sun, Y., Ruehl, C. R., and Setyan, A.: Effect of aqueous-phase processing
675 on aerosol chemistry and size distributions in Fresno, California, during wintertime, Environ.
676 Chem., 9, 221-235, 10.1071/EN11168, 2012a.

677 Ge, X. L., Setyan, A., Sun, Y., and Zhang, Q.: Primary and secondary organic aerosols in
678 Fresno, California during wintertime: Results from high resolution aerosol mass spectrometry,
679 J. Geophys. Res. - Atmos., 117, D19301, 10.1029/2012jd018026, 2012b.

680 Ghan, S. J., and Schwartz, S. E.: Aerosol properties and processes: A path from field and
681 laboratory measurements to global climate models, Bull. Am. Meteorol. Soc., 88, 1059-1083,
682 10.1175/bams-88-7-1059, 2007.

683 Han, T., Xu, W., Chen, C., Liu, X., Wang, Q., Li, J., Zhao, X., Du, W., Wang, Z., and Sun, Y.:
684 Chemical apportionment of aerosol optical properties during the Asia-Pacific Economic
685 Cooperation summit in Beijing, China, J. Geophys. Res. - Atmos., 120, 12,281-212,295,
686 10.1002/2015JD023918, 2015.

687 He, L. Y., Huang, X.-F., Xue, L., Hu, M., Lin, Y., Zheng, J., Zhang, R., and Zhang, Y.-H.:
688 Submicron aerosol analysis and organic source apportionment in an urban atmosphere in
689 Pearl River Delta of China using high-resolution aerosol mass spectrometry, J. Geophys. Res.
690 - Atmos., 116, D12304, 10.1029/2010jd014566, 2011.

691 Heald, C. L., Kroll, J. H., Jimenez, J. L., Docherty, K. S., DeCarlo, P. F., Aiken, A. C., Chen,
692 Q., Martin, S. T., Farmer, D. K., and Artaxo, P.: A simplified description of the evolution of
693 organic aerosol composition in the atmosphere, Geophys. Res. Lett., 37, L08803,
694 10.1029/2010gl042737, 2010.

695 Hu, J., Ying, Q., Wang, Y., and Zhang, H.: Characterizing multi-pollutant air pollution in
696 China: Comparison of three air quality indices, Environ. Int., 84, 17-25,
697 10.1016/j.envint.2015.06.014, 2015.

698 Hu, W. W., Hu, M., Yuan, B., Jimenez, J. L., Tang, Q., Peng, J. F., Hu, W., Shao, M., Wang,
699 M., Zeng, L. M., Wu, Y. S., Gong, Z. H., Huang, X. F., and He, L. Y.: Insights on organic
700 aerosol aging and the influence of coal combustion at a regional receptor site of central
701 eastern China, Atmos. Chem. Phys., 13, 10095-10112, 10.5194/acp-13-10095-2013, 2013.

702 Hu, X., Zhang, Y., Ding, Z. H., Wang, T. J., Lian, H. Z., Sun, Y. Y., and Wu, J. C.:
703 Bioaccessibility and health risk of arsenic and heavy metals (Cd, Co, Cr, Cu, Ni, Pb, Zn and
704 Mn) in TSP and $PM_{2.5}$ in Nanjing, China, Atmos. Environ., 57, 146-152,
705 10.1016/j.atmosenv.2012.04.056, 2012.

706 Huang, X.-F., Xue, L., Tian, X.-D., Shao, W.-W., Sun, T.-L., Gong, Z.-H., Ju, W.-W., Jiang, B.,
707 Hu, M., and He, L.-Y.: Highly time-resolved carbonaceous aerosol characterization in Yangtze
708 River Delta of China: composition, mixing state and secondary formation, Atmos. Environ.,
709 10.1016/j.atmosenv.2012.09.059, 2012a.

710 Huang, X. F., He, L. Y., Hu, M., Canagaratna, M. R., Sun, Y., Zhang, Q., Zhu, T., Xue, L.,
711 Zeng, L. W., Liu, X. G., Zhang, Y. H., Jayne, J. T., Ng, N. L., and Worsnop, D. R.: Highly
712 time-resolved chemical characterization of atmospheric submicron particles during 2008
713 Beijing Olympic Games using an Aerodyne High-Resolution Aerosol Mass Spectrometer,
714 Atmos. Chem. Phys., 10, 8933-8945, 10.5194/acp-10-8933-2010, 2010.

715 Huang, X. F., He, L. Y., Hu, M., Canagaratna, M. R., Kroll, J. H., Ng, N. L., Zhang, Y. H., Lin,
716 Y., Xue, L., Sun, T. L., Liu, X. G., Shao, M., Jayne, J. T., and Worsnop, D. R.:
717 Characterization of submicron aerosols at a rural site in Pearl River Delta of China using an
718 Aerodyne High-Resolution Aerosol Mass Spectrometer, Atmos. Chem. Phys., 11, 1865-1877,
719 10.5194/acp-11-1865-2011, 2011.

720 Huang, X. F., He, L. Y., Xue, L., Sun, T. L., Zeng, L. W., Gong, Z. H., Hu, M., and Zhu, T.:
721 Highly time-resolved chemical characterization of atmospheric fine particles during 2010
722 Shanghai World Expo, Atmos. Chem. Phys., 12, 4897-4907, 10.5194/acp-12-4897-2012,
723 2012b.

724 Jayne, J. T., Leard, D. C., Zhang, X., Davidovits, P., Smith, K. A., Kolb, C. E., and Worsnop,
725 D. R.: Development of an Aerosol Mass Spectrometer for Size and Composition Analysis of
726 Submicron Particles, Aerosol Sci. Tech., 33, 49 - 70, 10.1016/S0021-8502(98)00158-X, 2000.

727 Jiang, Q., Sun, Y. L., Wang, Z., and Yin, Y.: Aerosol composition and sources during the
728 Chinese Spring Festival: fireworks, secondary aerosol, and holiday effects, Atmos. Chem.
729 Phys., 15, 6023-6034, 10.5194/acp-15-6023-2015, 2015.

730 Jimenez, J. L., Jayne, J. T., Shi, Q., Kolb, C. E., Worsnop, D. R., Yourshaw, I., Seinfeld, J. H.,
731 Flagan, R. C., Zhang, X. F., Smith, K. A., Morris, J. W., and Davidovits, P.: Ambient aerosol
732 sampling using the Aerodyne Aerosol Mass Spectrometer, J. Geophys. Res. - Atmos., 108,
733 8425, 10.1029/2001jd001213, 2003.

734 Jimenez, J. L., Canagaratna, M. R., Donahue, N. M., Prevot, A. S. H., Zhang, Q., Kroll, J. H.,
735 DeCarlo, P. F., Allan, J. D., Coe, H., Ng, N. L., Aiken, A. C., Docherty, K. S., Ulbrich, I. M.,
736 Grieshop, A. P., Robinson, A. L., Duplissy, J., Smith, J. D., Wilson, K. R., Lanz, V. A.,
737 Hueglin, C., Sun, Y. L., Tian, J., Laaksonen, A., Raatikainen, T., Rautiainen, J., Vaattovaara, P.,
738 Ehn, M., Kulmala, M., Tomlinson, J. M., Collins, D. R., Cubison, M. J., Dunlea, E. J.,
739 Huffman, J. A., Onasch, T. B., Alfarra, M. R., Williams, P. I., Bower, K., Kondo, Y., Schneider,
740 J., Drewnick, F., Borrmann, S., Weimer, S., Demerjian, K., Salcedo, D., Cottrell, L., Griffin,
741 R., Takami, A., Miyoshi, T., Hatakeyama, S., Shimono, A., Sun, J. Y., Zhang, Y. M., Dzepina,
742 K., Kimmel, J. R., Sueper, D., Jayne, J. T., Herndon, S. C., Trimborn, A. M., Williams, L. R.,
743 Wood, E. C., Middlebrook, A. M., Kolb, C. E., Baltensperger, U., and Worsnop, D. R.:
744 Evolution of organic aerosols in the atmosphere, Science, 326, 1525-1529,
745 10.1126/science.1180353, 2009.

746 Kong, S. F., Li, L., Li, X. X., Yin, Y., Chen, K., Liu, D. T., Yuan, L., Zhang, Y. J., Shan, Y. P.,
747 and Ji, Y. Q.: The impacts of firework burning at the Chinese Spring Festival on air quality:
748 insights of tracers, source evolution and aging processes, Atmos. Chem. Phys., 15, 2167-2184,
749 10.5194/acp-15-2167-2015, 2015.

750 Lee, A. K. Y., Hayden, K. L., Herckes, P., Leaitch, W. R., Liggio, J., Macdonald, A. M., and
751 Abbatt, J. P. D.: Characterization of aerosol and cloud water at a mountain site during WACS
752 2010: secondary organic aerosol formation through oxidative cloud processing, Atmos. Chem.
753 Phys., 12, 7103-7116, 10.5194/acp-12-7103-2012, 2012.

754 Lee, B. P., Li, Y. J., Yu, J. Z., Louie, P. K. K., and Chan, C. K.: Physical and chemical
755 characterization of ambient aerosol by HR-ToF-AMS at a suburban site in Hong Kong during
756 springtime 2011, J. Geophys. Res. - Atmos., n/a-n/a, 10.1002/jgrd.50658, 2013.

757 Li, Y. J., Lee, B. P., Su, L., Fung, J. C. H., and Chan, C. K.: Seasonal characteristics of fine
758 particulate matter (PM) based on high-resolution time-of-flight aerosol mass spectrometric
759 (HR-ToF-AMS) measurements at the HKUST Supersite in Hong Kong, Atmos. Chem. Phys.,
760 15, 37-53, 10.5194/acp-15-37-2015, 2015.

761 Malm, W. C., and Day, D. E.: Estimates of aerosol species scattering characteristics as a

762 function of relative humidity, Atmos. Environ., 35, 2845-2860,
763 10.1016/S1352-2310(01)00077-2, 2001.

764 Middlebrook, A. M., Bahreini, R., Jimenez, J. L., and Canagaratna, M. R.: Evaluation of
765 Composition-Dependent Collection Efficiencies for the Aerodyne Aerosol Mass Spectrometer
766 using Field Data, Aerosol Sci. Tech., 46, 258-271, 10.1080/02786826.2011.620041, 2012.

767 Mohr, C., DeCarlo, P. F., Heringa, M. F., Chirico, R., Slowik, J. G., Richter, R., Reche, C.,
768 Alastuey, A., Querol, X., Seco, R., Peñuelas, J., Jiménez, J. L., Crippa, M., Zimmermann, R.,
769 Baltensperger, U., and Prévôt, A. S. H.: Identification and quantification of organic aerosol
770 from cooking and other sources in Barcelona using aerosol mass spectrometer data, Atmos.
771 Chem. Phys., 12, 1649-1665, 10.5194/acp-12-1649-2012, 2012.

772 Mohr, C., DeCarlo, P. F., Heringa, M. F., Chirico, R., Richter, R., Crippa, M., Querol, X.,
773 Baltensperger, U., and Prévôt, A. S. H.: Spatial Variation of Aerosol Chemical Composition
774 and Organic Components Identified by Positive Matrix Factorization in the Barcelona Region,
775 Environ. Sci. Technol., 49, 10421-10430, 10.1021/acs.est.5b02149, 2015.

776 Ng, N. L., Canagaratna, M. R., Zhang, Q., Jimenez, J. L., Tian, J., Ulbrich, I. M., Kroll, J. H.,
777 Docherty, K. S., Chhabra, P. S., Bahreini, R., Murphy, S. M., Seinfeld, J. H., Hildebrandt, L.,
778 Donahue, N. M., DeCarlo, P. F., Lanz, V. A., Prevot, A. S. H., Dinar, E., Rudich, Y., and
779 Worsnop, D. R.: Organic aerosol components observed in Northern Hemispheric datasets
780 from Aerosol Mass Spectrometry, Atmos. Chem. Phys., 10, 4625-4641,
781 10.5194/acp-10-4625-2010, 2010.

782 Ng, N. L., Herndon, S. C., Trimborn, A., Canagaratna, M. R., Croteau, P. L., Onasch, T. B.,
783 Sueper, D., Worsnop, D. R., Zhang, Q., Sun, Y. L., and Jayne, J. T.: An Aerosol Chemical
784 Speciation Monitor (ACSM) for Routine Monitoring of the Composition and Mass
785 Concentrations of Ambient Aerosol, Aerosol Sci. Tech., 45, 770-784,
786 10.1080/02786826.2011.560211, 2011.

787 Onasch, T. B., Trimborn, A., Fortner, E. C., Jayne, J. T., Kok, G. L., Williams, L. R.,
788 Davidovits, P., and Worsnop, D. R.: Soot particle aerosol mass spectrometer: Development,
789 validation, and initial application, Aerosol Sci. Tech., 46, 804-817,
790 10.1080/02786826.2012.663948, 2012.

791 Paatero, P., and Tapper, U.: Positive matrix factorization: A non-negative factor model with
792 optimal utilization of error estimates of data values, Environmetrics, 5, 111-126,
793 10.1002/env.3170050203, 1994.

794 Pope, C. A., and Dockery, D. W.: Health Effects of Fine Particulate Air Pollution: Lines that
795 Connect, J. Air Waste Manage., 56, 709-742, 10.1080/10473289.2006.10464485, 2006.

796 Pöschl, U.: Atmospheric Aerosols: Composition, Transformation, Climate and Health Effects,
797 Angewandte Chemie International Edition, 44, 7520-7540, 10.1002/anie.200501122, 2005.

798 Seinfeld, J. H., and Pandis, S. N.: Atmospheric Chemistry and Physics: From Air Pollution to
799 Climate Change, John Wiley & Sons, New York, 2006.

800 Setyan, A., Zhang, Q., Merkel, M., Knighton, W. B., Sun, Y., Song, C., Shilling, J. E., Onasch,
801 T. B., Herndon, S. C., Worsnop, D. R., Fast, J. D., Zaveri, R. A., Berg, L. K., Wiedensohler, A.,
802 Flowers, B. A., Dubey, M. K., and Subramanian, R.: Characterization of submicron particles
803 influenced by mixed biogenic and anthropogenic emissions using high-resolution aerosol
804 mass spectrometry: results from CARES, Atmos. Chem. Phys., 12, 8131-8156,
805 10.5194/acp-12-8131-2012, 2012.

806 Shen, G. F., Yuan, S. Y., Xie, Y. N., Xia, S. J., Li, L., Yao, Y. K., Qiao, Y. Z., Zhang, J., Zhao,
807 Q. Y., Ding, A. J., Li, B., and Wu, H. S.: Ambient levels and temporal variations of $PM_{2.5}$ and
808 PM_{10} at a residential site in the mega-city, Nanjing, in the western Yangtze River Delta, China,
809 J. Environ. Sci. Health., Part A, 49, 171-178, 10.1080/10934529.2013.838851, 2014.

810 Shen, X. J., Sun, J. Y., Zhang, X. Y., Zhang, Y. M., Zhang, L., Che, H. C., Ma, Q. L., Yu, X.
811 M., Yue, Y., and Zhang, Y. W.: Characterization of submicron aerosols and effect on visibility
812 during a severe haze-fog episode in Yangtze River Delta, China, Atmos. Environ., 120,
813 307-316, 10.1016/j.atmosenv.2015.09.011, 2015.

814 Sun, Y., Jiang, Q., Wang, Z., Fu, P., Li, J., Yang, T., and Yin, Y.: Investigation of the Sources
815 and Evolution Processes of Severe Haze Pollution in Beijing in January 2013, J. Geophys.
816 Res. - Atmos., 2014JD021641, 10.1002/2014JD021641, 2014.

817 Sun, Y. L., Zhang, Q., Schwab, J. J., Demerjian, K. L., Chen, W. N., Bae, M. S., Hung, H. M.,
818 Hogrefe, O., Frank, B., Rattigan, O. V., and Lin, Y. C.: Characterization of the sources and
819 processes of organic and inorganic aerosols in New York city with a high-resolution
820 time-of-flight aerosol mass apectrometer, Atmos. Chem. Phys., 11, 1581-1602,
821 10.5194/acp-11-1581-2011, 2011.

822 Sun, Y. L., Du, W., Wang, Q., Zhang, Q., Chen, C., Chen, Y., Chen, Z., Fu, P., Wang, Z., Gao,
823 Z., and Worsnop, D. R.: Real-Time Characterization of Aerosol Particle Composition above
824 the Urban Canopy in Beijing: Insights into the Interactions between the Atmospheric
825 Boundary Layer and Aerosol Chemistry, Environ. Sci. Technol., 49, 11340-11347,
826 10.1021/acs.est.5b02373, 2015a.

827 Sun, Y. L., Wang, Z. F., Du, W., Zhang, Q., Wang, Q. Q., Fu, P. Q., Pan, X. L., Li, J., Jayne, J.,
828 and Worsnop, D. R.: Long-term real-time measurements of aerosol particle composition in
829 Beijing, China: seasonal variations, meteorological effects, and source analysis, Atmos. Chem.
830 Phys., 15, 10149-10165, 10.5194/acp-15-10149-2015, 2015b.

831 Sun, Y. L., Wang, Z., Wild, O., Xu, W., Chen, C., Fu, P., Du, W., Zhou, L., Zhang, Q., Han, T.,
832 Wang, Q., Pan, X., Zheng, H., Li, J., Guo, X., Liu, J., and Worsnop, D. R.: “APEC Blue”:
833 Secondary Aerosol Reductions from Emission Controls in Beijing, Sci. Rep., 6, 20668,
834 10.1038/srep20668, 2016.

835 Tang, L., Yu, H., Ding, A., Zhang, Y., Qin, W., Wang, Z., Chen, W., Hua, Y., and Yang, X.:
836 Regional contribution to PM1 pollution during winter haze in Yangtze River Delta, China, Sci.
837 Total Environ., 541, 161-166, 10.1016/j.scitotenv.2015.05.058, 2016.

838 Ulbrich, I. M., Canagaratna, M. R., Zhang, Q., Worsnop, D. R., and Jimenez, J. L.:
839 Interpretation of organic components from Positive Matrix Factorization of aerosol mass
840 spectrometric data, Atmos. Chem. Phys., 9, 2891-2918, 10.5194/acp-9-2891-2009, 2009.

841 Wang, G. H., Niu, S. L., Liu, C., and Wang, L. S.: Identification of dicarboxylic acids and
842 aldehyde of PM_{10} and $PM_{2.5}$ aerosols in Nanjing, China, Atmos. Environ., 36, 1941-1950,
843 10.1016/s1352-2310(02)00180-2, 2002.

844 Wang, G. H., Wang, H., Yu, Y. J., Gao, S. X., Feng, J. F., Gao, S. T., and Wang, L. S.:
845 Chemical characterization of water-soluble components of PM_{10} and $PM_{2.5}$ atmospheric
846 aerosols in five locations of Nanjing, China, Atmos. Environ., 37, 2893-2902,
847 10.1016/s1352-2310(03)00271-1, 2003.

848 Wang, G. H., Kawamura, K., Xie, M. J., Hu, S. Y., Cao, J. J., An, Z. S., Waston, J. G., and
849 Chow, J. C.: Organic molecular compositions and size distributions of Chinese summer and
850 autumn aerosols from Nanjing: Characteristic haze event caused by wheat straw burning,
851 Environ. Sci. Technol., 43, 6493-6499, 10.1021/es803086g, 2009.

852 Wang, G. H., Chen, C. L., Li, J. J., Zhou, B. H., Xie, M. J., Hu, S. Y., Kawamura, K., and
853 Chen, Y.: Molecular composition and size distribution of sugars, sugar-alcohols and
854 carboxylic acids in airborne particles during a severe urban haze event caused by wheat straw
855 burning, Atmos. Environ., 45, 2473-2479, 10.1016/j.atmosenv.2011.02.045, 2011.

856 Wang, J., Onasch, T. B., Ge, X., Collier, S., Zhang, Q., Sun, Y., Yu, H., Chen, M., Prévôt, A. S.
857 H., and Worsnop, D. R.: Observation of Fullerene Soot in Eastern China, Environ. Sci.
858 Technol. Lett., 10.1021/acs.estlett.6b00044, 2016a.

859 Wang, Q., Sun, Y., Jiang, Q., Du, W., Sun, C., Fu, P., and Wang, Z.: Chemical composition of
860 aerosol particles and light extinction apportionment before and during the heating season in
861 Beijing, China, J. Geophys. Res. - Atmos., 120, 2015JD023871, 10.1002/2015JD023871,
862 2015.

863 Wang, Q., Zhao, J., Du, W., Ana, G., Wang, Z., Sun, L., Wang, Y., Zhang, F., Li, Z., Ye, X.,
864 and Sun, Y.: Characterization of submicron aerosols at a suburban site in central China, Atmos
865 Environ, 131, 115-123, http://dx.doi.org/10.1016/j.atmosenv.2016.01.054, 2016b.

866 Wexler, A. S., and Johnston, M. V.: What have we learned from highly time-resolved
867 measurements during EPA's Supersites program,and related studies?, J. Air Waste Manage.,
868 58, 303-319, 10.3155/1047-3289.58.2.303, 2008.

869 Xu, J., Zhang, Q., Chen, M., Ge, X., Ren, J., and Qin, D.: Chemical composition, sources, and
870 processes of urban aerosols during summertime in northwest China: insights from

high-resolution aerosol mass spectrometry, Atmos. Chem. Phys., 14, 12593-12611, 10.5194/acp-14-12593-2014, 2014.

Xu, W. Q., Sun, Y. L., Chen, C., Du, W., Han, T. T., Wang, Q. Q., Fu, P. Q., Wang, Z. F., Zhao, X. J., Zhou, L. B., Ji, D. S., Wang, P. C., and Worsnop, D. R.: Aerosol composition, oxidation properties, and sources in Beijing: results from the 2014 Asia-Pacific Economic Cooperation summit study, Atmos. Chem. Phys., 15, 13681-13698, 10.5194/acp-15-13681-2015, 2015.

Yan, J., Chen, L., Lin, Q., Li, Z., Chen, H., and Zhao, S.: Chemical characteristics of submicron aerosol particles during a long-lasting haze episode in Xiamen, China, Atmos. Environ., 113, 118-126, 10.1016/j.atmosenv.2015.05.003, 2015.

Yang, H., Yu, J. Z., Ho, S. S. H., Xu, J. H., Wu, W. S., Wan, C. H., Wang, X. D., Wang, X. R., and Wang, L. S.: The chemical composition of inorganic and carbonaceous materials in $PM_{2.5}$ in Nanjing, China, Atmos. Environ., 39, 3735-3749, 10.1016/j.atmosenv.2005.03.010, 2005.

Yang, L.-X., Wang, D.-c., Cheng, S.-h., Wang, Z., Zhou, Y., Zhou, X.-h., and Wang, W.-x.: Influence of meteorological conditions and particulate matter on visual range impairment in Jinan, China, Sci. Total Environ., 383, 164-173, 10.1016/j.scitotenv.2007.04.042, 2007.

Yeung, M. C., Lee, B. P., Li, Y. J., and Chan, C. K.: Simultaneous HTDMA and HR-ToF-AMS measurements at the HKUST Supersite in Hong Kong in 2011, J. Geophys. Res. - Atmos., 2013JD021146, 10.1002/2013JD021146, 2014.

Young, D. E., Kim, H., Parworth, C., Zhou, S., Zhang, X., Cappa, C. D., Seco, R., Kim, S., and Zhang, Q.: Influences of emission sources and meteorology on aerosol chemistry in a polluted urban environment: results from DISCOVER-AQ California, Atmos. Chem. Phys. Discuss., 2015, 35057-35115, 10.5194/acpd-15-35057-2015, 2015.

Yu, L., Smith, J., Laskin, A., Anastasio, C., Laskin, J., and Zhang, Q.: Chemical characterization of SOA formed from aqueous-phase reactions of phenols with the triplet excited state of carbonyl and hydroxyl radical, Atmos. Chem. Phys., 14, 13801-13816, 10.5194/acp-14-13801-2014, 2014.

Zhang, J. K., Sun, Y., Liu, Z. R., Ji, D. S., Hu, B., Liu, Q., and Wang, Y. S.: Characterization of submicron aerosols during a month of serious pollution in Beijing, 2013, Atmos. Chem. Phys., 14, 2887-2903, 10.5194/acp-14-2887-2014, 2014.

Zhang, J. K., Wang, L. L., Wang, Y. H., and Wang, Y. S.: Submicron aerosols during the Beijing Asia–Pacific Economic Cooperation conference in 2014, Atmos. Environ., 124, Part B, 224-231, 10.1016/j.scitotenv.2007.04.042, 2016a.

Zhang, Q., Alfarra, M. R., Worsnop, D. R., Allan, J. D., Coe, H., Canagaratna, M. R., and Jimenez, J. L.: Deconvolution and quantification of hydrocarbon-like and oxygenated organic aerosols based on aerosol mass spectrometry, Environ. Sci. Technol., 39, 4938-4952, 10.1021/Es048568l, 2005.

907 Zhang, Q., Jimenez, J. L., Canagaratna, M. R., Allan, J. D., Coe, H., Ulbrich, I., Alfarra, M. R.,
908 Takami, A., Middlebrook, A. M., Sun, Y. L., Dzepina, K., Dunlea, E., Docherty, K., DeCarlo,
909 P. F., Salcedo, D., Onasch, T., Jayne, J. T., Miyoshi, T., Shimono, A., Hatakeyama, S.,
910 Takegawa, N., Kondo, Y., Schneider, J., Drewnick, F., Borrmann, S., Weimer, S., Demerjian,
911 K., Williams, P., Bower, K., Bahreini, R., Cottrell, L., Griffin, R. J., Rautiainen, J., Sun, J. Y.,
912 Zhang, Y. M., and Worsnop, D. R.: Ubiquity and dominance of oxygenated species in organic
913 aerosols in anthropogenically-influenced Northern Hemisphere midlatitudes, Geophys. Res.
914 Lett., 34, L13801, 10.1029/2007gl029979, 2007a.

915 Zhang, Q., Jimenez, J. L., Worsnop, D. R., and Canagaratna, M.: A case study of urban
916 particle acidity and its influence on secondary organic aerosol, Environ. Sci. Technol., 41,
917 3213-3219, 10.1021/Es061812j, 2007b.

918 Zhang, Q., Jimenez, J., Canagaratna, M., Ulbrich, I., Ng, N., Worsnop, D., and Sun, Y.:
919 Understanding atmospheric organic aerosols via factor analysis of aerosol mass spectrometry:
920 a review, Anal. Bioanal. Chem., 401, 3045-3067, 10.1007/s00216-011-5355-y, 2011.

921 Zhang, Y. J., Tang, L. L., Wang, Z., Yu, H. X., Sun, Y. L., Liu, D., Qin, W., Canonaco, F.,
922 Prévôt, A. S. H., Zhang, H. L., and Zhou, H. C.: Insights into characteristics, sources, and
923 evolution of submicron aerosols during harvest seasons in the Yangtze River delta region,
924 China, Atmos. Chem. Phys., 15, 1331-1349, 10.5194/acp-15-1331-2015, 2015.

925 Zhang, Y. J., Tang, L., Yu, H., Wang, Z., Sun, Y., Qin, W., Chen, W., Chen, C., Ding, A., Wu,
926 J., Ge, S., Chen, C., and Zhou, H.-c.: Chemical composition, sources and evolution processes
927 of aerosol at an urban site in Yangtze River Delta, China during wintertime, Atmos. Environ.,
928 10.1016/j.atmosenv.2015.08.017, 2016b.
929
930
931

Atmos. Chem. Phys. Discuss., doi:10.5194/acp-2016-226, 2016
Manuscript under review for journal Atmos. Chem. Phys.
Published: 21 March 2016

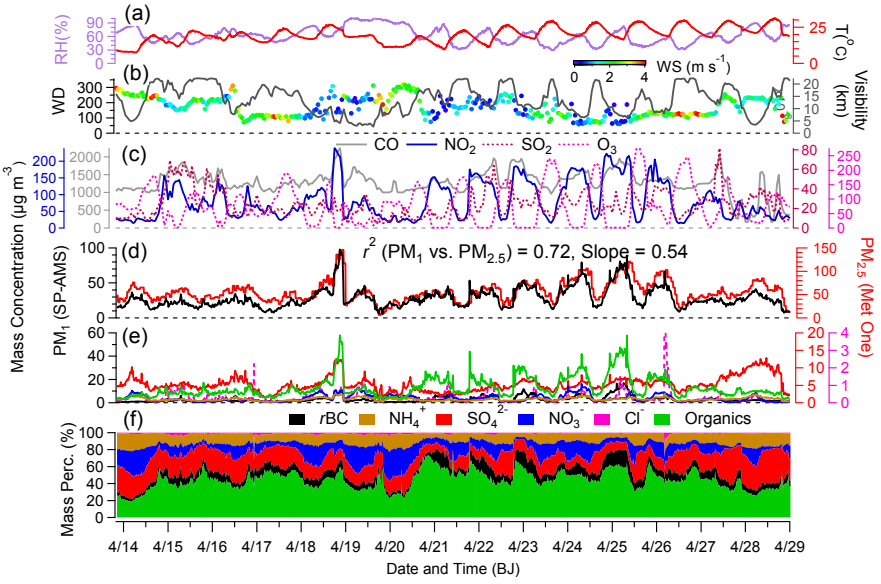

Figure 1. Time series of (a) relative humidity (RH) and temperature (T), (b) wind direction (WD) colored by wind speed (WS, m s^{-1}) and visibility (km), (c) mass concentrations of CO, NO_2, SO_2 and O_3 (hourly data), (d) mass concentrations of PM_1 measured by the SP-AMS, and $PM_{2.5}$ measured by the co-located Met One $PM_{2.5}$ analyzer, (e) mass concentrations of *r*BC, ammonium, sulfate, nitrate, chloride and organics, and (f) mass contributions (%) of the six PM_1 components (BJ, Beijing).

Atmos. Chem. Phys. Discuss., doi:10.5194/acp-2016-226, 2016
Manuscript under review for journal Atmos. Chem. Phys.
Published: 21 March 2016

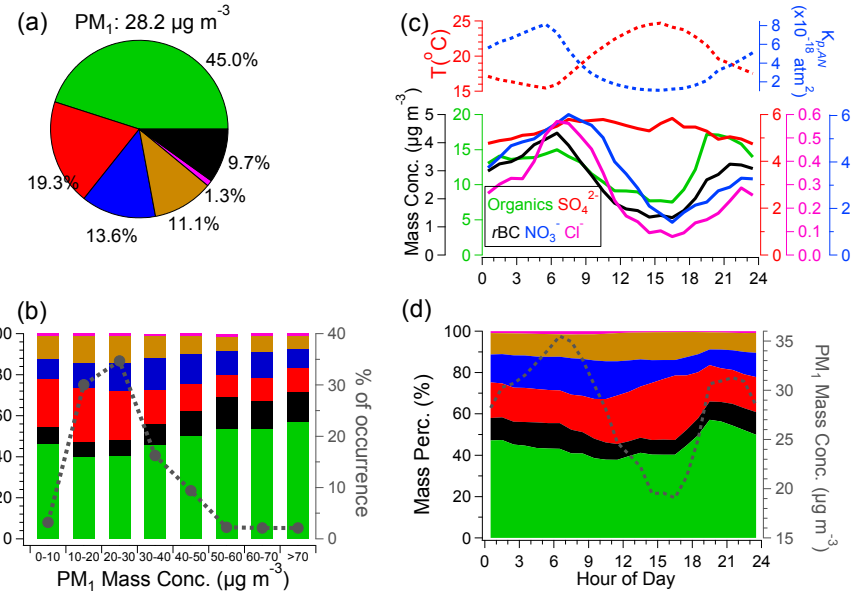

Figure 2. (a) Campaign-averaged mass contributions of organics, sulfate, nitrate, ammonium, chloride and *r*BC to the total PM_1, (b) mass percentages of the six PM_1 species (left *y*-axis) and, fractions of the number of data points to the total number of data points for PM_1 at different concentration bins (right *y*-axis), (c) diurnal patterns of mass concentrations of the major PM_1 species (bottom panel), temperature (top panel, left *y*-axis), and the equilibrium constant ($K_{p,AN}$) of NH_4NO_3 (top panel, right *y*-axis) ($K_{p,AN} = K_{p,AN}(298)exp\left\{a\left(\frac{298}{T}-1\right)+b\left[1+ln\left(\frac{298}{T}\right)-\frac{298}{T}\right]\right\}$, for reaction $NH_3(g) + HNO_3(g) \leftrightarrow NH_4NO_3(p)$. $K_{p,AN}(298)$ is the equilibrium constant at 298 K (3.36×10^{-16} atm^2), a = 75.11, and b = -13.5 (Seinfeld and Pandis, 2006)), (d) diurnal variations of mass fractional contributions of the six PM_1 species (left *y*-axis), and the PM_1 mass concentrations (right *y*-axis).

Atmos. Chem. Phys. Discuss., doi:10.5194/acp-2016-226, 2016
Manuscript under review for journal Atmos. Chem. Phys.
Published: 21 March 2016

Atmospheric Chemistry and Physics Discussions

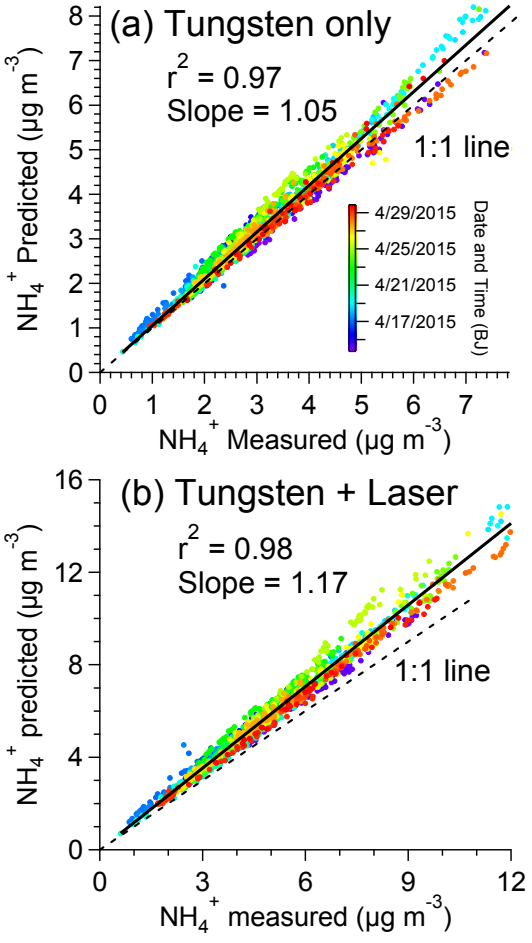

Figure 3. Scatter plots of the predicted NH_4^+ *vs.* measured NH_4^+ concentrations (colored by time), in the case of (a) tungsten vaporizer only, and (b) dual-vaporizers (tungsten + laser). The predicted values were calculated according to the formula: NH_4^+ predicted = $18\times(2\times SO_4^{2-}/96 + NO_3^-/62 + Cl^-/35.5)$ (Zhang et al., 2007b).

Atmos. Chem. Phys. Discuss., doi:10.5194/acp-2016-226, 2016
Manuscript under review for journal Atmos. Chem. Phys.
Published: 21 March 2016

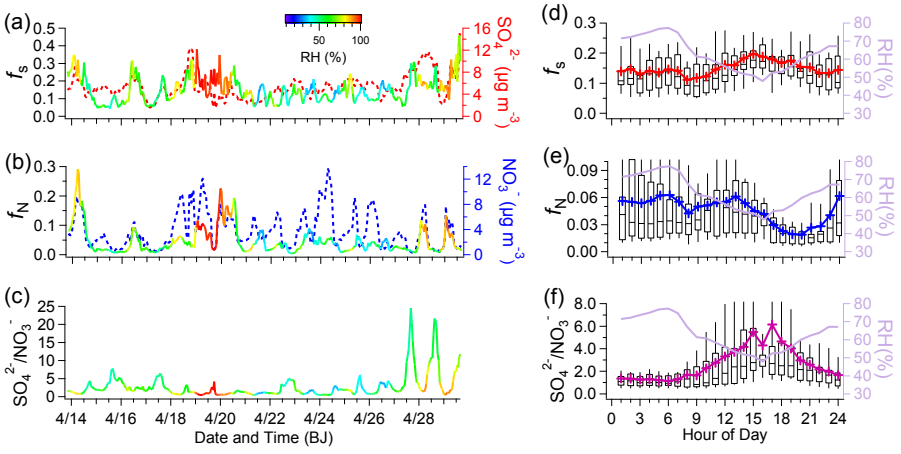

Figure 4. Time series of (a) sulfur oxidation ratio, $f_S = nSO_4^{2-}/(nSO_4^{2-} + nSO_2)$, and sulfate, (b) nitrogen oxidation ratio, $f_N = nNO_3^-/(nNO_3^- + nNO_2)$, and nitrate, and (c) mass ratios of sulfate to nitrate (f_S, f_N and SO_4^{2-}/NO_3^- are colored by the relative humidity (RH) values), diurnal variations of (d) f_S, (e) f_N, and (f) SO_4^{2-}/NO_3^- and RH (the lines and cross symbols indicate the mean values, the lines in the boxes indicate the median values, the upper and lower boundaries of the boxes indicate the 75th and 25th percentiles, and the whiskers above and below the boxes indicate the 90th and 10th percentiles).

Atmos. Chem. Phys. Discuss., doi:10.5194/acp-2016-226, 2016
Manuscript under review for journal Atmos. Chem. Phys.
Published: 21 March 2016

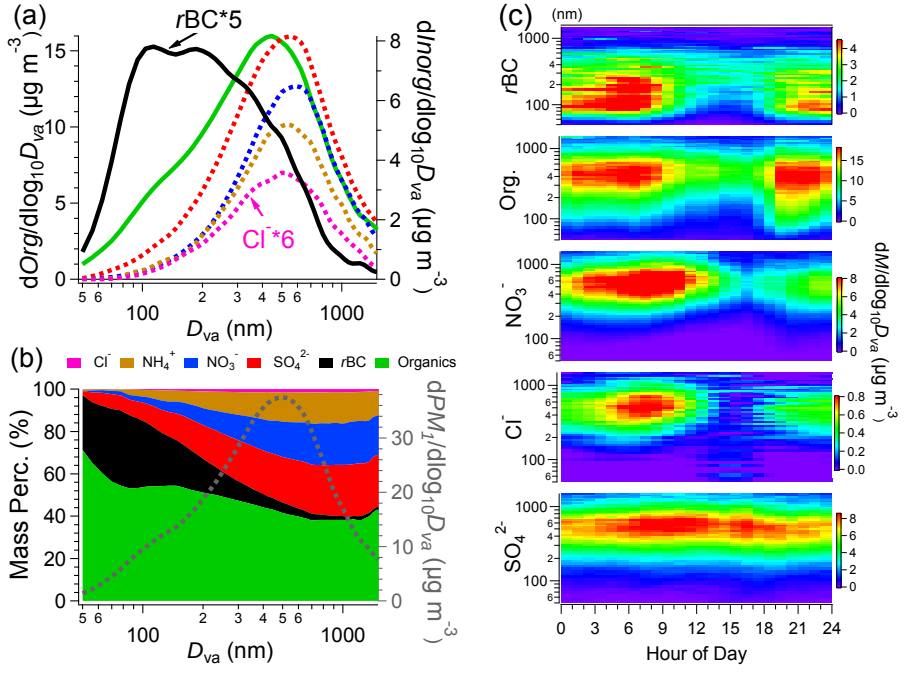

Figure 5. (a) Mass-based average size distributions of organics, *r*BC (left *y*-axis), sulfate, nitrate, chloride and ammonium (right *y*-axis) (D_{va}, vacuum aerodynamic diameter), (b) fractional contributions of the six PM_1 species as a function of particle size (left *y*-axis), and size distribution of total PM_1 (right *y*-axis), (c) diurnal profiles of the size distributions of *r*BC, organics, nitrate, chloride and sulfate.

Atmos. Chem. Phys. Discuss., doi:10.5194/acp-2016-226, 2016
Manuscript under review for journal Atmos. Chem. Phys.
Published: 21 March 2016

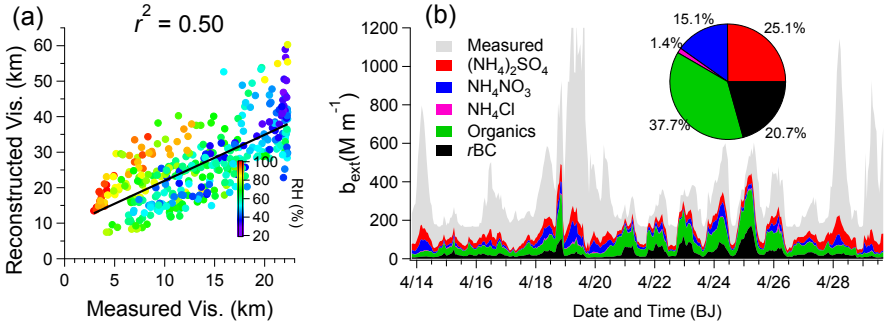

Figure 6. (a) Scatter plot of reconstructed *vs.* measured visibility (colored by RH), (b) light extinction coefficients derived from measured visibility (grey), and reconstructed from SP-AMS measured ammonium sulfate, ammonium nitrate, ammonium chloride, organics and *r*BC using the IMPROVE method. The inset pie shows the relative contributions of the five species to the light extinction of PM_1.

Atmos. Chem. Phys. Discuss., doi:10.5194/acp-2016-226, 2016
Manuscript under review for journal Atmos. Chem. Phys.
Published: 21 March 2016

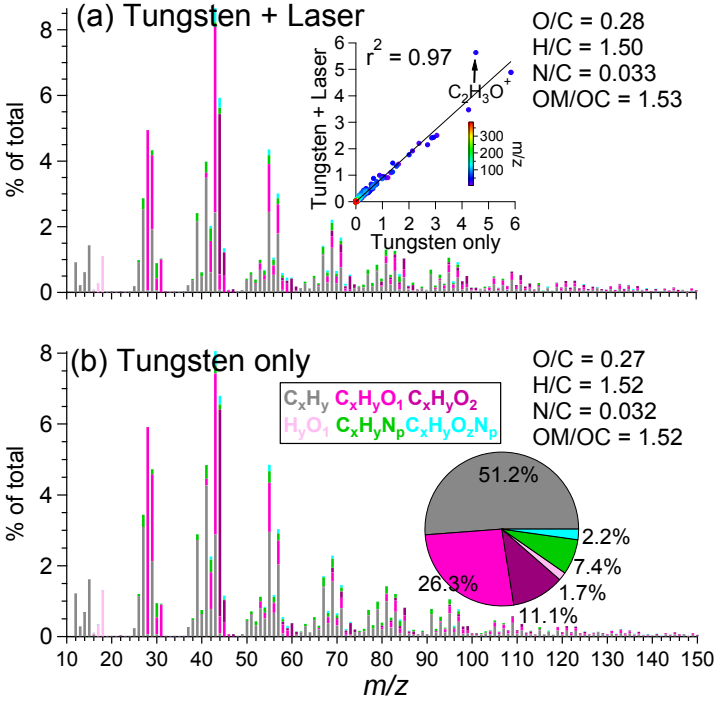

Figure 7. Campaign-averaged high resolution mass spectra of OA colored by six ion categories, in the case of (a) dual-vaporizers (tungsten + laser) (the inset scatter plot compares the spectral similarity between (a) and (b)), and (b) tungsten vaporizer only (the inset pie shows the relative contributions of six ion categories to the total OA).

Atmos. Chem. Phys. Discuss., doi:10.5194/acp-2016-226, 2016
Manuscript under review for journal Atmos. Chem. Phys.
Published: 21 March 2016

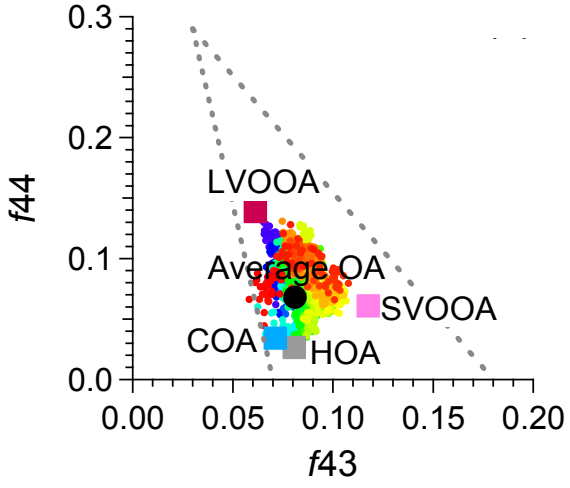

Figure 8. Triangle plot of *f*44 *vs.* *f*43 for all OA (colored by time), and the four OA factors identified by the PMF analyses.

Atmos. Chem. Phys. Discuss., doi:10.5194/acp-2016-226, 2016
Manuscript under review for journal Atmos. Chem. Phys.
Published: 21 March 2016

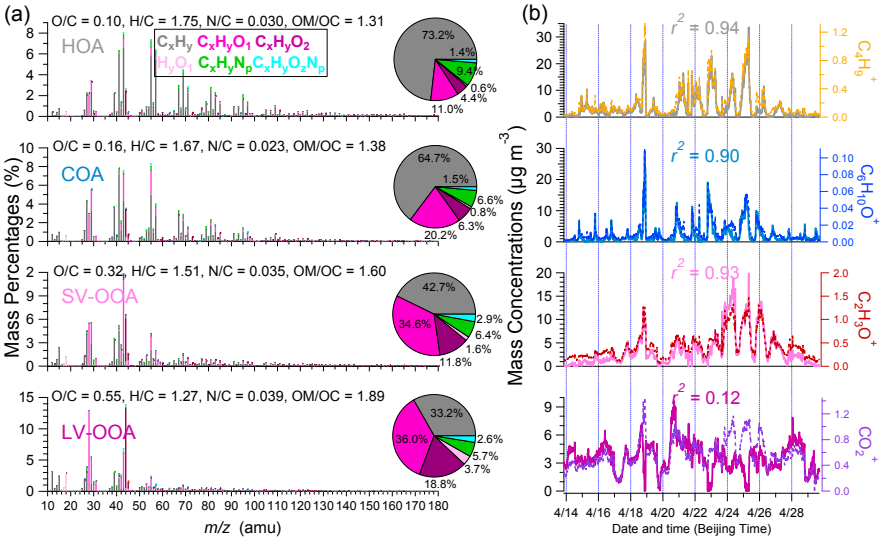

Figure 9. (a) High resolution mass spectra of hydrocarbon-like OA (HOA), cooking-related OA (COA), semi-volatile oxygenated OA (SV-OOA), and low volatility oxygenated OA (LV-OOA) colored by six ion categories (the four inset pies show the relative contributions of the six ion categories to the four OA factors, respectively), (b) time series of the four OA factors and corresponding tracer ions.

Atmos. Chem. Phys. Discuss., doi:10.5194/acp-2016-226, 2016
Manuscript under review for journal Atmos. Chem. Phys.
Published: 21 March 2016

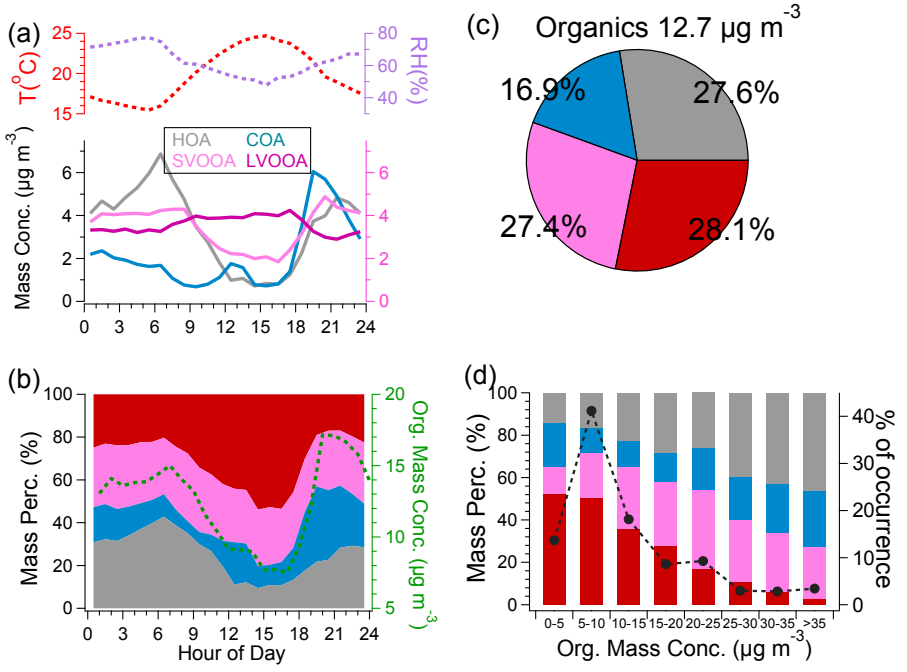

Figure 10. (a) Diurnal cycles of mass concentrations of the four OA factors (bottom panel), temperature (top panel, left *y*-axis) and RH (top panel, right *y*-axis), (b) diurnal variations of mass contributions of the four OA factors (left *y*-axis), and the total OA mass concentrations (right *y*-axis), (c) campaign-averaged mass contributions of the four OA factors to the total OA mass, and (d) mass contributions of the four OA factors (left *y*-axis), and the fractions of the number of data points to the total number of data points for the OA at different concentration ranges (right *y*-axis).

Atmos. Chem. Phys. Discuss., doi:10.5194/acp-2016-226, 2016
Manuscript under review for journal Atmos. Chem. Phys.
Published: 21 March 2016

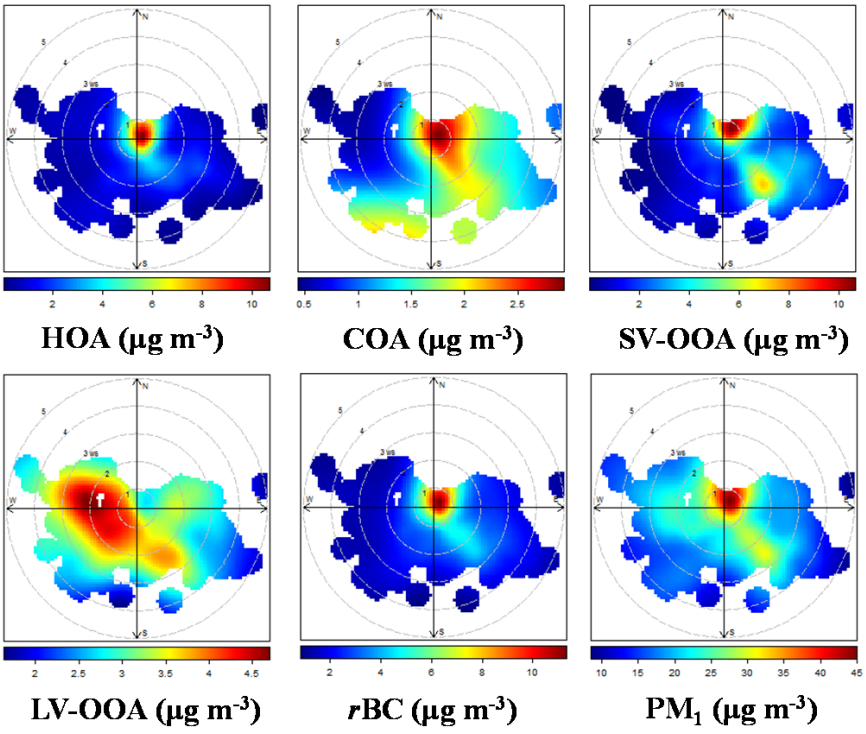

Figure 11. Bivariate polar plots of HOA, COA, SV-OOA, LV-OOA, *r*BC and PM_1 (the color scale shows the concentration of each species, and the radical scale shows the wind speed that increases outward from the center).

Atmos. Chem. Phys. Discuss., doi:10.5194/acp-2016-226, 2016
Manuscript under review for journal Atmos. Chem. Phys.
Published: 21 March 2016

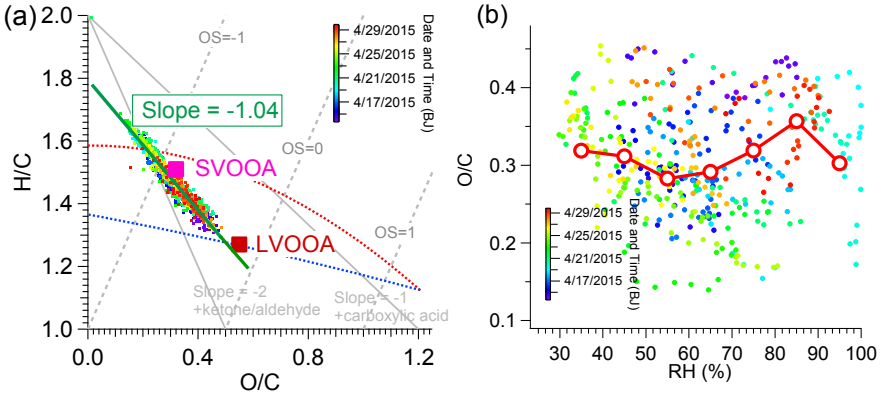

Figure 12. (a) Van Krevelen diagram of H/C *vs.* O/C ratios for all OA data colored by time, the blue and red dashed lines correspond to the right and left grey dashed lines in the *f*44 vs. f43 triangle plot of Fig. 8, the grey lines represents the addition of a particular functional group to an aliphatic carbon (Heald et al., 2010), (b) scatter plot of O/C *vs.* RH (colored by time), the circles represents the average O/C values of the RH bins (10% increment).

Atmos. Chem. Phys. Discuss., doi:10.5194/acp-2016-226, 2016
Manuscript under review for journal Atmos. Chem. Phys.
Published: 21 March 2016

Atmospheric Chemistry and Physics Discussions

1038 Table 1. Correlation coefficients (Pearson's r^2) between the mass spectral profiles of
1039 the OA factors identified in this work with the corresponding factors identified in
1040 Beijing (2013 Winter) (Sun et al., 2015a), Lanzhou (2014 Summer) ((Xu et al., 2014)),
1041 and Fresno (2010 Winter) (Ge et al., 2012b).
1042

Nanjing (2015 Spring)	High resolution MS (r^2)		
	Beijing (2013 Winter)	Lanzhou (2012 Summer)	Fresno (2010 Winter)*
HOA	0.92	0.90	0.98
COA	0.93	0.94	0.93
SV-OOA	0.68	0.75	0.90
LV-OOA	0.91	0.98	0.87
	Unit mass resolution MS (r^2)		
HOA	0.92	0.91	0.99
COA	0.96	0.96	0.95
SV-OOA	0.70	0.74	0.91
LV-OOA	0.90	0.98	0.89

1043 *Note the Fresno (2010 Winter) study only identified one OOA factor, we thus
1044 compared both SV-OOA and LV-OOA in this study with it.

Atmos. Chem. Phys. Discuss., doi:10.5194/acp-2016-226, 2016
Manuscript under review for journal Atmos. Chem. Phys.
Published: 21 March 2016

Atmospheric Chemistry and Physics Discussions

Table 2. Correlation coefficients (Pearson's *r*) between the time series of the four OA factors with the gas-phase species (hourly data) and other PM_1 components (15-min data), and the correlation coefficients between the diurnal data.

Pearson's *r*	Temp.(T)	CO	NO_2	SO_2	O_3	SO_4^{2-}	NO_3^-	Cl^-	*r*BC
	Hourly data					15-min data			
HOA	-0.14	0.71	0.77	0.13	-0.54	0.15	0.26	0.45	0.92
COA	0.11	0.50	0.58	-0.06	-0.22	0.19	0.07	0.08	0.61
SVOOA	0.19	0.41	0.70	0.14	-0.21	0.11	0.49	0.25	0.70
LVOOA	0.069	-0.2	-0.18	0.06	0.14	0.23	0.11	0.01	-0.22
	Diurnal data								
HOA	-0.94	0.86	0.86	0.66	-0.96	-0.35	0.72	0.82	0.99
COA	-0.15	0.28	0.59	-0.24	-0.24	-0.57	-0.33	-0.25	0.19
SVOOA	-0.85	0.86	0.94	0.58	-0.90	-0.51	0.53	0.61	0.89
LVOOA	0.76	-0.58	-0.83	-0.27	0.77	0.72	-0.26	-0.33	-0.75